Stability of Finite Element Models for Distributed-Parameter Optimization and Topology Design

Chandrashekhar S. Jog and Robert B. Haber
Department of Theoretical and Applied Mechanics,
University of Illinois at Urbana-Champaign,
Urbana, Illinois, USA

Abstract:

We address a problem of numerical instability that is often encountered in finite element solutions of distributed-parameter optimization and variable-topology shape design problems. We show that the cause of this problem is numerical rather than physical in nature. We consider a two-field, distributed-parameter optimization problem involving a design field and a response field, and show that the optimization problem corresponds to a mixed variational problem. An improper selection of the discrete function spaces for these two fields leads to grid-scale anomalies in the numerical solutions to optimization problems, similar to those that are sometimes encountered in mixed formulations of the Stokes problem. We present a theoretical framework to explain the cause of these anomalies and present stability conditions for discrete models. The general theoretical framework is specialized to analyze the stability of specific optimization problems, and stability results for various mixed finite element models are presented. We propose patch tests that are useful in identifying unstable elements.

1. Introduction

This paper is concerned with a form of numerical instability that commonly occurs in finite element solution procedures for distributed-parameter optimization problems. These problems involve the optimal selection of one or more scalar or tensor-valued design fields defined on a specified domain. For example, one might attempt to determine the optimal thickness distribution for an elastic plate to control the local stress state or the plate's natural frequencies. Although the physics of a given problem might imply a regular solution, optimization procedures based on discrete models often generate anomalies in the design field at the length scale of the numerical grid. These anomalies can take the form of "checkerboard" disturbances, wherein the discrete solution for the design field alternately overestimates and underestimates the expected continuum solution in adjacent elements.

Checkerboard anomalies are commonly observed in published solutions to variable-topology shape optimization problems ([1]-[7]). In these problems, the goal is to determine an optimal distribution of a fixed volume of material within a candidate domain to extremize an objective function, such as the compliance of an elastic structure, under prescribed loading and support conditions. Instead of using boundary representations to describe the structure's geometry, it is common practice to introduce a bulk density parameter ρ such that a value of 1 denotes solid material and a value of 0 denotes void. The elastic material properties are expressed as a continuous function of ρ (often according to a homogenized microstructural model that arises in relaxed formulations of the topology design problem—see [2], [3], [8]). The shape design problem then involves the determination of an optimal distribution of ρ (or an alternative collection of microstructural design parameters) over the candidate domain. A penalty against intermediate values of ρ may be introduced to ensure that the domain is primarily occupied by either solid material or void. Thus, the variable-topology shape optimization shape optimization problem is commonly treated as a distributed parameter optimization problem.

The checkerboard patterns that appear in topology design solutions are not associated with any specific material model. They have been observed with material models derived

from rank-2 laminates ([1], [2]), from partial relaxations based on rectangular holes in square cells ([3]-[6]), and from simple variable-density models [7].

To illustrate the problem, consider the candidate region, supports and loading conditions shown in Figure 1. We seek the minimum compliance design using an optimized rank-2 laminate to model the material properties (see [2] for details). When we discretize the problem using 8-node quadrilateral displacement elements and a uniform density per element, we obtain the smoothly-varying density field shown in Figure 2. (Actually, this element is mildly unstable; see section 5 for a detailed discussion.) However, when we use a 4-node displacement interpolation and a uniform density per element, we observe checkerboard modes in the solution, as shown in Figure 3. Similar checkerboard modes are observed in the numerical examples presented by Suzuki et al., who use a microstructure model based on rectangular holes in square cells (see Figure 15 in [6]), and in the examples of Rozvany et al., who use a variable-thickness model (see Figure 11 in [7]).

Similar checkerboard anomalies have been observed by researchers in biomechanics in studies of adaptive bone remodeling. Here the objective is to simulate a natural process in which the density of living bone is increased or decreased in response to local, mechanical stimuli. For example, Weinans et al. [9] propose a model in which the time rate of bone density is given by

$$\dot{\rho} = B\,(W - k)\,, \tag{1}$$

in which B is a scalar constant, W is the strain energy density and k is a constant corresponding to a reference value of the strain energy density. An isotropic material model, with Young's modulus given by $E = c\rho^{\gamma}$ ($c = 100$ MPa $(\text{g cm}^{-3})^{-2}$; $\gamma = 2$) and a Poisson's ratio of 0.3 was assumed. According to equation (1), the bone remodeling process achieves a steady state ($\dot{\rho} = 0$) when the strain energy distribution is uniform at the reference value k. This is similar to the uniform-energy-density optimality criterion for minimum compliance design for a fixed volume of material. Thus, adaptive bone remodeling is closely related to distributed parameter optimization. Indeed, Weinans et al. also report

grid-scale, checkerboard anomalies in their finite element calculations. Similar discontinuous solutions were reported by Goldstein el al. in a study of bone-ingrowth around porous-coated implants [10].

Jog, Haber and Bendsøe suggest that the anomalies encountered in the variable-topology design problem are related to the spurious modes that sometimes pollute mixed finite element solutions ([1], [2]). They point out that weak formulations of the topology design problem yield a mixed variational form, involving independent displacement and density fields, not unlike mixed formulations used to model incompressible elasticity and Stokes flow. They also demonstrate that certain combinations of density and displacement interpolation functions generate finite element solutions that are free of grid-scale anomalies. The observation that finite element solutions based on single-field formulations of the design problem are free of anomalies [11] provides further evidence that the mixed finite element model is the source of the problem. While the numerical evidence supporting the explanation of checkerboard designs as spurious modes in a mixed finite element model is strong, a detailed analysis of the problem has yet to appear in the literature. This paper seeks to present an explanation for checkerboards (and other related anomalies) in distributed-parameter optimization problems based on the theory of mixed finite element methods. The theory presented here provides insight into the cause of checkerboard anomalies as well as practical means to predict their occurrence and to avoid them.

The organization of the remainder of this paper is as follows. In Section 2, we present the general formulation of a distributed-parameter optimization problem that we will refer to in later sections of this work. We develop a mixed variational statement of the optimization problem and compare it to mixed formulations of the Stokes problem. We also develop incremental and discrete forms of the problem that are used in our subsequent analysis. In Section 3, we review selected aspects of the theory of mixed variational formulations. We present stability analyses for special cases of the distributed-parameter optimization problem in Sections 4 and 5 using the formulation developed in Section 2. Strategies for generating stable finite element solutions are presented in Section 6. In Section 7, we present the conclusions of this paper.

2. A distributed-parameter optimization problem

This section introduces a distributed-parameter optimization problem associated with the minimum compliance design of an elastic continuum. The problem is first presented in a general form to illustrate the common structure that links the special cases to be investigated in subsequent sections. We begin with a statement of the governing equations and the optimization problem. The weak forms of the stationary conditions are developed, yielding a nonlinear mixed variational problem. Rather than analyzing the stability of the nonlinear problem directly, we instead consider the linearized, incremental form of the mixed variational problem and the discrete matrix equations that derive from it.

2.1. Governing equations

Let Ω be an open domain whose boundary Γ is composed of two open, disjoint regions, $\Gamma = \overline{\Gamma_u \cup \Gamma_t}$. The domain Ω contains a linear elastic material with a variable bulk density specified by the function ρ: $\Omega \rightarrow \Re$. (In some applications, ρ is a variable-thickness parameter, rather than a material density.) The value of the strain energy density function for the elastic material, $W(\varepsilon, \rho)$, depends on the local values of the strain and bulk density. We assume small deformation behavior and a single, static loading case. The governing equations are:

$$\nabla \cdot \sigma + \boldsymbol{b} = 0 \text{ in } \Omega, \tag{2}$$

$$\varepsilon(\boldsymbol{u}) = \frac{1}{2}[\nabla \boldsymbol{u} + (\nabla \boldsymbol{u})^t] \text{ in } \Omega, \tag{3}$$

$$\sigma = \frac{\partial W}{\partial \varepsilon} \text{ in } \Omega, \tag{4}$$

$$\boldsymbol{t} = \sigma \cdot \boldsymbol{n} \text{ on } \Gamma, \tag{5}$$

$$\boldsymbol{u} = 0 \text{ on } \Gamma_u, \tag{6}$$

$$\boldsymbol{t} = \bar{\boldsymbol{t}} \text{ on } \Gamma_t. \tag{7}$$

ε is the strain tensor, $\boldsymbol{u}$ is the displacement vector, σ is the stress tensor, $\boldsymbol{b}$ is the prescribed body force vector, $\boldsymbol{t}$ is the traction vector, $\boldsymbol{n}$ is the unit normal vector to the surface Γ, and $\bar{\boldsymbol{t}}$ is a vector of prescribed tractions.

2.2. *Optimization problem (P0)*

Our objective is to find an optimal density distribution that minimizes the compliance of the elastic structure subject to an equality constraint on the total volume of material, $\int_\Omega \rho d\Omega = \bar{V}$, and upper and lower-bound constraints on the density, $0 < \rho_{min} \le \rho \le 1$. The latter constraint derives from the interpretation that $\rho = 1$ corresponds to solid material and $\rho = 0$ denotes void. The compliance objective may be augmented with an optional penalty on intermediate values of density between the solid and void states. Recall that the compliance is equal to twice the additive inverse of the potential energy ([1], [2])

$$\Pi(\boldsymbol{u}, \rho) = \int_\Omega W(\varepsilon, \rho)\, d\Omega - \int_{\Gamma_t} (\bar{\boldsymbol{t}} \cdot \boldsymbol{u})\, d\Gamma - \int_\Omega (\boldsymbol{b} \cdot \boldsymbol{u})\, d\Omega. \tag{8}$$

Define $V_u = \{\boldsymbol{u} \in H^1(\Omega) : \boldsymbol{u} = 0 \text{ on } \Gamma_u\}$ and $V_\rho = L_\infty(\Omega)$, and assume that equations (3)-(5) are strictly enforced. Then the optimization problem is stated as

Problem P0:

Let ρ_{min}: $0 < \rho_{min} < 1$, $\alpha \ge 0$ and $\bar{V} > 0$ be given. Find $(\boldsymbol{u}^*, \rho^*) \in V_u \times V_\rho$ that solves

$$\sup_{\rho \in V_\rho} \inf_{\boldsymbol{u} \in V_u} \Pi(\boldsymbol{u}, \rho) - \lambda\left(\int_\Omega \rho d\Omega - \bar{V}\right) - \alpha \int_\Omega \rho\,(1-\rho)\, d\Omega, \tag{9}$$

subject to $\rho_{min} \le \rho \le 1$ in Ω; where λ is the Lagrange multiplier associated with the constraint $\int_\Omega \rho d\Omega = \bar{V}$.

Some comments on problem P0 are in order at this point. The inner *inf* operation is responsible for weak enforcement of the equilibrium equation (2) and the traction boundary condition (7). The penalty term can be used to approximate a $0-1$ integer programming problem in ρ when we specify $\alpha > 0$. This is useful in variable-topology shape optimization problems where the objective is to partition Ω into regions of solid material and void ([11]-[13]). Alternatively, we can set $\alpha = 0$ and manipulate the strain energy density function W to achieve an implicit penalty on intermediate densities (see Section 5).

The question of whether the functional in problem P0 is linear or nonlinear in ρ turns out to be a key issue in our stability analysis. In the former case, we must have $\alpha = 0$ and the strain energy density function must be linear in ρ. The optimal design of a variable-thickness elastic plate is a common example of this class of problem (here ρ is understood as a thickness parameter). Topology optimization generally involves the nonlinear case, due either to a nonzero penalty term or a nonlinear dependence of W on ρ. These two cases are treated in detail in Sections 4 and 5.

2.3. *Stationary conditions and the variational problem (POv)*

We next present variational forms of the stationary conditions for problem P0. A solution to problem P0 must solve the following problem.

Problem P0v:

Let ρ_{min}: $0 < \rho_{min} < 1$, $\alpha \geq 0$ and $\bar{V} > 0$ be given. Find $(\boldsymbol{u}, \rho) \in V_u \times V_\rho$ such that

$$\int_\Omega \varepsilon^t(\boldsymbol{v})\, \sigma d\Omega = \int_{\Gamma_t} (\bar{\boldsymbol{t}} \cdot \boldsymbol{v})\, d\Gamma + \int_\Omega (\boldsymbol{b} \cdot \boldsymbol{v})\, d\Omega \quad \forall \boldsymbol{v} \in V_u, \tag{10}$$

$$\int_\Omega \frac{\partial W}{\partial \rho} q d\Omega - \alpha \int_\Omega (1 - 2\rho)\, q d\Omega = \lambda \int_\Omega q d\Omega \quad \forall q \in V_\rho, \tag{11}$$

subject to $\rho_{min} \leq \rho \leq 1$ in Ω; where λ is the Lagrange multiplier associated with the constraint $\int_{\Omega} \rho d\Omega = \bar{V}$. The fields v and q represent, respectively, variations of the displacement and density fields.

Equation (10) is the familiar virtual work equation, while equation (11) is a weak form of the optimality criterion,

$$\frac{\partial W}{\partial \rho} - \lambda - \alpha(1 - 2\rho) = 0. \tag{12}$$

The stationary conditions, (10) and (11), are necessary, but not sufficient, for a solution to problem P0. Convexity of the potential energy ensures that the second-order Kuhn-Tucker conditions are satisfied for the displacement field. However, the second-order conditions for the density field must be checked independently (see Section 5).

It is evident that problem P0 corresponds to a mixed variational problem involving the independent fields $\boldsymbol{u}$ and ρ. A rough analogy can be drawn between problem P0 and mixed formulations of the Stokes problem [14]. That is, the displacement and density fields in problem P0 correspond to the velocity and pressure field in the Stokes problem. Similarly, the equilibrium equations in the two problems are analogous, and the optimality condition (12) corresponds to the incompressibility constraint in the Stokes problem. It is well known that discrete approximations of mixed variational problems may be subject to numerical instabilities even when the continuum problem is well-behaved [15]. In particular, mixed finite element solutions to the Stokes problem can exhibit grid-scale anomalies that are strikingly similar to those encountered in distributed parameter optimization problems. This observation motivates our analysis of checkerboard designs and other grid-scale anomalies within the theoretical framework of mixed finite element methods, as developed by (among others) Babuska, Brezzi and Fortin [15].

2.4. *The linearized, incremental problem (P0i)*

Although there are similarities between our distributed-parameter optimization problem and familiar mixed variational problems, such as the Stokes problem, there are also some significant differences. For example, problem P0 is nonlinear, while the Stokes problem is linear. Since the stability theory for nonlinear mixed variational problems is less developed than the theory for linear problems, our study focuses on a linearized, incremental form of problem P0. The incremental problem corresponds to a single step within an iterative solution procedure for the nonlinear problem. If each iterative update is numerically stable and the overall iterative process is convergent, then we can argue that the overall scheme is well behaved. The linearized incremental form of problem P0v is presented next.

Let $\boldsymbol{u}^0$ and ρ^0 represent the current estimates of the displacement and density fields, and let $\delta\boldsymbol{u}$ and $\delta\rho$ represent increments in the two fields. Carrying out the linear expansion of σ and $\frac{\partial W}{\partial \rho}$, we get

$$\sigma = \sigma^0 + \left(\frac{\partial \sigma}{\partial \varepsilon}\right)^0 \varepsilon(\delta \boldsymbol{u}) + \left(\frac{\partial \sigma}{\partial \rho}\right)^0 \delta\rho, \tag{13}$$

$$\frac{\partial W}{\partial \rho} = \left(\frac{\partial W}{\partial \rho}\right)^0 + \left(\frac{\partial^2 W}{\partial \varepsilon \partial \rho}\right)^0 \varepsilon(\delta \boldsymbol{u}) + \left(\frac{\partial^2 W}{\partial \rho^2}\right)^0 \delta\rho. \tag{14}$$

The superscript 0 in equations (13) and (14) indicates that the quantity is evaluated at the current estimate of the solution, $(\boldsymbol{u}^0, \rho^0)$. The volume constraint takes the form $\int_\Omega (\rho^0 + \delta\rho)\, d\Omega = \bar{V}$. Assuming that the current density distribution ρ_0 satisfies the volume constraint, we get $\int_\Omega \delta\rho\, d\Omega = 0$. Substituting equations (13) and (14) in equations (10) and (11), and collecting all known terms on the right hand side, we obtain the following incremental problem.

Problem P0i:

Let ρ_{min}: $0 < \rho_{min} < 1$, $\alpha \geq 0$, $\bar{V} > 0$, $\boldsymbol{u}^0 \in V_u$ and $\rho^0 \in V_\rho$: $\int_\Omega \rho^0 d\Omega = \bar{V}$ be given. Find $(\delta \boldsymbol{u}, \delta\rho) \in V_u \times V_\rho$ such that

$$\int_\Omega \varepsilon^t(v) \left(\frac{\partial \sigma}{\partial \varepsilon}\right)^0 \varepsilon(\delta \boldsymbol{u})\, d\Omega + \int_\Omega \varepsilon^t(v) \left(\frac{\partial \sigma}{\partial \rho}\right)^0 \delta\rho\, d\Omega = \langle f, v\rangle \quad \forall v \in V_u, \tag{15}$$

$$\int_\Omega \left(\frac{\partial^2 W}{\partial \varepsilon \partial \rho}\right)^0 \varepsilon(\delta \boldsymbol{u})\, q\, d\Omega + \int_\Omega \left[\left(\frac{\partial^2 W}{\partial \rho^2}\right)^0 + 2\alpha\right] \delta\rho q\, d\Omega = \langle g, q\rangle \quad \forall q \in V_\rho, \tag{16}$$

subject to $\rho_{min} - \rho^0 \leq \delta\rho \leq 1 - \rho^0$, where

$$\langle f, v\rangle = \int_{\Gamma_t} (\bar{\boldsymbol{t}} \cdot v)\, d\Gamma + \int_\Omega (\boldsymbol{b} \cdot v)\, d\Omega - \int_\Omega \varepsilon^t(v)\, \sigma^0 d\Omega, \tag{17}$$

$$\langle g, q\rangle = \lambda \int_\Omega q\, d\Omega + \alpha \int_\Omega (1 - 2\rho^0)\, q\, d\Omega - \int_\Omega \left(\frac{\partial W}{\partial \rho}\right)^0 q\, d\Omega, \tag{18}$$

and λ is the Lagrange multiplier associated with the constraint $\int_\Omega \delta\rho\, d\Omega = 0$.

2.5. *The discrete problem (P0d)*

Our ultimate goal is to study the stability of finite element approximations to problem P0. Accordingly, we next develop the discrete form of the incremental optimization problem. We begin by introducing the following finite element approximations for the field variables in the incremental problem.

$$\begin{aligned} \delta \boldsymbol{u} &= N_u \delta \hat{\boldsymbol{u}} \qquad & \boldsymbol{u}^0 &= N_u \hat{\boldsymbol{u}}^0 \qquad & v &= N_u \hat{v} \\ \delta\rho &= N_\rho \delta\hat{\rho} \qquad & \rho^0 &= N_\rho \hat{\rho}^0 \qquad & q &= N_\rho \hat{q} \end{aligned} \tag{19}$$

N_u and $\delta\hat{u} \in \Re^{n_u}$ are the matrix of basis functions and the incremental parameter vector for the displacement field, while N_ρ and $\delta\hat{\rho} \in \Re^{n_\rho}$ are the corresponding items for the density field. The parameter vectors $\hat{u}^0$ and $\hat{\rho}^0$ contain the current estimates of the discrete solution. We define the matrices A, B^t and H, and the vectors $\hat{f}$ and $\hat{g}$ as

$$A \equiv \int_\Omega B_u^t C^0 B_u d\Omega, \tag{20}$$

$$B^t \equiv \int_\Omega B_u^t \left(\frac{\partial \sigma}{\partial \rho}\right)^0 N_\rho d\Omega, \tag{21}$$

$$H \equiv \int_\Omega \left[\left(\frac{\partial^2 W}{\partial \rho^2}\right)^0 + 2\alpha\right] N_\rho^t N_\rho d\Omega, \tag{22}$$

$$\hat{f} \equiv \int_{\Gamma_t} N_u^t \bar{t} d\Gamma + \int_\Omega N_u^t b d\Omega - \int_\Omega B_u^t \sigma^0 d\Omega, \tag{23}$$

$$\hat{g} \equiv \lambda \int_\Omega N_\rho^t d\Omega + \alpha \int_\Omega (1 - 2\rho^0) N_\rho^t d\Omega - \int_\Omega \left(\frac{\partial W}{\partial \rho}\right)^0 N_\rho^t d\Omega, \tag{24}$$

in which B_u is the strain-displacement matrix, and $C^0 = \left(\frac{\partial \sigma}{\partial \varepsilon}\right)^0$ is the material stiffness matrix. We now present the discrete form of problem P0i.

Problem P0d:

Let ρ_{min}: $0 < \rho_{min} < 1$, $\alpha \geq 0$, $\bar{V} > 0$, $\hat{u}^0 \in \Re^{n_u}$ and $\hat{\rho}^0 \in \Re^{n_\rho}$: $\int_\Omega N_\rho d\Omega \hat{\rho}^0 = \bar{V}$ be given.

Find $(\delta\hat{u}, \delta\hat{\rho}) \in \Re^{n_u} \times \Re^{n_\rho}$ that solves

$$\begin{bmatrix} A & B^t \\ B & H \end{bmatrix} \begin{Bmatrix} \delta\hat{u} \\ \delta\hat{\rho} \end{Bmatrix} = \begin{Bmatrix} \hat{f} \\ \hat{g} \end{Bmatrix}, \tag{25}$$

subject to $\rho_{min} - \hat{\rho}_\beta^0 \le \delta\hat{\rho}_\beta \le 1 - \hat{\rho}_\beta^0$; $\beta = 1, n_\rho$; where $\boldsymbol{A}$, $\boldsymbol{B}$, $\boldsymbol{H}$, $\hat{\boldsymbol{f}}$ and $\hat{\boldsymbol{g}}$ are defined as above and λ is the Lagrange multiplier associated with the constraint, $\int_\Omega N_\rho d\Omega \delta\hat{\rho} = 0$.

The vectors $\hat{\boldsymbol{f}}$ and $\hat{\boldsymbol{g}}$ derive from the terms $\langle f, v \rangle$ and $\langle g, q \rangle$, respectively, and represent the residuals of the equilibrium and optimality conditions given by equations (10) and (11). The matrix $\boldsymbol{A}$ is the stiffness matrix, and $-\boldsymbol{B}^t$ is a matrix whose columns are the *pseudoload vectors* corresponding to the elements of $\delta\hat{\rho}$, as defined in the direct differentiation method of design sensitivity analysis [16]. The matrix in equation (25) is the Hessian of the Lagrangian with respect to $(\hat{\boldsymbol{u}}, \hat{\rho})$.

The side constraints on $\delta\hat{\rho}$ are sufficient to enforce $\rho_{min} \le \rho \le 1$ in Ω for finite element models with constant-per-element and bilinear-per-element density fields; however, they are not sufficient for higher-order elements. In the stability analysis of Section 5, we are concerned with the properties of the partition of the Hessian that is associated with elements of $\delta\hat{\rho}$ for which the side constraints are not active. To simplify matters, we will henceforth assume that the side constraints are inactive for all of the density degrees of freedom.

The remainder of this paper is devoted to a study of the stability of the discrete, incremental problem (P0d) within the general theoretical framework of mixed variational problems. The next section contains a brief review of the relevant theory. In section 4, we consider the special case where $\boldsymbol{H} = \boldsymbol{O}$, which occurs whenever the functional in problem P0 is linear in ρ. Section 5 addresses the more general situation where $\boldsymbol{H}$ may be nonzero.

3. A review of the theory of mixed variational problems

In this section, we review results regarding the existence and uniqueness of solutions to continuum formulations of mixed variational problems. Then we consider discrete

approximations of the continuum problem, typically based on mixed finite element models, and discuss the conditions under which discrete models yield a reasonable approximation to the continuum solution. We follow the development of Brezzi and Fortin [15].

3.1. Abstract formulation of a mixed variational problem

In order to treat mixed finite element formulations of the Stokes flow problem or the standard Dirichlet problem under a general framework, Brezzi and Fortin consider the following abstract formulation:

Let V be a Hilbert space with the scalar product $(\cdot,\cdot)_V$, and let $a(\cdot,\cdot)$ be a continuous bilinear form on $V \times V$. This bilinear form defines a continuous operator $A : V \to V'$ (a prime denotes a dual space):

$$\langle Au, v\rangle_{V' \times V} = a(u, v) \quad \forall (u, v) \in V \times V. \tag{26}$$

Let Q be another Hilbert space, with scalar product $(\cdot,\cdot)_Q$, and let $b(v, q)$ be a continuous bilinear form defined on $V \times Q$. This bilinear form defines a linear operator $B : V \to Q'$ and its transpose $B^t : Q \to V'$:

$$\langle Bv, q\rangle_{Q' \times Q} = \langle v, B^t q\rangle_{V \times V'} = b(v, q) \quad \forall (v, q) \in V \times Q. \tag{27}$$

Now consider the following variational problem. Let $f \in V'$ and $g \in Q'$ be given. The problem is to find $(u, \rho) \in V \times Q$ such that

$$\begin{aligned} a(u, v) + b(v, \rho) &= \langle f, v\rangle_{V' \times V} \quad \forall v \in V \\ b(u, q) &= \langle g, q\rangle_{Q' \times Q} \quad \forall q \in Q \end{aligned} \tag{28}$$

Equations (28) can also be written as

$$\begin{aligned} Au + B^t \rho &= f \text{ in } V' \\ Bu &= g \text{ in } Q' \end{aligned} \tag{29}$$

We define the kernel of B (denoted by $Ker\ B$) as

$$Ker\ B = \{v \in V : Bv = 0 \text{ in } Q'\}, \tag{30}$$

and the image of B (denoted by $Im\ B$) as

$$Im\ B = \{q \in Q' : q = Bv\}. \tag{31}$$

The following theorem addresses the existence and uniqueness properties of the mixed variational problem.

Theorem 1

Let $a(\cdot,\cdot)$ and $b(\cdot,\cdot)$ be continuous bilinear forms on $V \times V$ and $V \times Q$. Let the range of the operator B associated with $b(\cdot,\cdot)$ be closed in Q', that is, there exists $k_0 > 0$ such that

$$\sup_{v \in V} \frac{b(v,q)}{\|v\|_V} \geq k_0 \|q\|_{Q/(KerB^t)}. \tag{32}$$

If moreover $a(\cdot,\cdot)$ is coercive on $Ker\ B$, i.e., there exists $\alpha_0 > 0$ such that

$$a(v_0, v_0) \geq \alpha_0 \|v_0\|_V^2 \quad \forall v_0 \in Ker\ B, \tag{33}$$

then there exists a solution (u, ρ) to equations (28) for any $f \in V'$ and for any $g \in Im\ B$. The first element u is unique, and the second element ρ is defined modulo an element of $Ker\ B^t$.

3.2. Approximation using a mixed finite element method

We now state results corresponding to Theorem 1 for the existence and uniqueness of solutions to finite-dimensional approximations of problem (28); as in, for example, a mixed finite element method. In the following development, we restrict our attention to the case where the solution (u, ρ) is unique (i. e., $Ker\ B^t = \{0\}$).

Let V_h and Q_h be finite-dimensional subspaces of V and Q, respectively. We are interested in finding a solution (u_h, ρ_h) in $V_h \times Q_h$ to

$$
\begin{aligned}
a(u_h, v_h) + b(v_h, \rho_h) &= \langle f, v_h \rangle_{V' \times V} \quad \forall v_h \in V_h \\
b(u_h, q_h) &= \langle g, q_h \rangle_{Q' \times Q} \quad \forall q \in Q_h
\end{aligned}
\tag{34}
$$

Introducing the basis functions ϕ and ψ for the spaces V_h and Q_h, we express the fields u_h, v_h, ρ_h and q_h in terms of the parameter vectors $\hat{u}$, $\hat{v}$, $\hat{\rho}$ and $\hat{q}$ as

$$
\begin{aligned}
u_h &= \phi \hat{u} \qquad \rho_h = \psi \hat{\rho} \\
v_h &= \phi \hat{v} \qquad q_h = \psi \hat{q}
\end{aligned}
\tag{35}
$$

Defining the matrices $\boldsymbol{A}$ and $\boldsymbol{B}$, and the vectors $\hat{f}$ and $\hat{g}$ as

$$
\begin{aligned}
A_{ij} &= a(\phi_j, \phi_i) \\
B_{ij} &= b(\phi_j, \psi_i) \\
\hat{f}_i &= \langle f, \phi_i \rangle \\
\hat{g}_i &= \langle g, \psi_i \rangle
\end{aligned}
\tag{36}
$$

the matrix forms of the equations (34) are given by

$$
\begin{aligned}
\boldsymbol{A}\hat{u} + \boldsymbol{B}^t \hat{\rho} &= \hat{f} \\
\boldsymbol{B}\hat{u} &= \hat{g}
\end{aligned}
\tag{37}
$$

or

$$
\begin{bmatrix} \boldsymbol{A} & \boldsymbol{B}^t \\ \boldsymbol{B} & \boldsymbol{O} \end{bmatrix} \begin{Bmatrix} \hat{u} \\ \hat{\rho} \end{Bmatrix} = \begin{Bmatrix} \hat{f} \\ \hat{g} \end{Bmatrix}. \tag{38}
$$

We next state a theorem regarding the existence and uniqueness of a solution (u_h, ρ_h) to equation (34). We first define the operator $B_h : V_h \to Q_h'$ and its transpose $B_h^t : Q_h \to V_h'$ as

$$
\langle B_h v_h, q_h \rangle_{Q_h' \times Q_h} = \langle v_h, B_h^t q_h \rangle_{V_h \times V_h'} = b(v_h, q_h). \tag{39}
$$

We also define the kernel of B_h^t as

$$Ker\ B_h^t = \{ q_h \in Q_h : B_h^t q_h = 0 \text{ in } V_h' \}. \tag{40}$$

Note that $Ker\ B^t = \{0\}$ does not imply $Ker\ B_h^t = \{0\}$.

Theorem 2

Assume that $a(\cdot,\cdot)$ is coercive on $Ker\ B_h$. That is, there exists $\alpha_0 > 0$ such that

$$a(v_{0h}, v_{0h}) \geq \alpha_0 \| v_{0h} \|_V^2 \quad \forall v_{0h} \in Ker\ B_h. \tag{41}$$

Also, assume there exists a k_0 such that the following *inf-sup* condition (known as the *Babuska-Brezzi* condition) holds for any conforming mesh:

$$k_h \geq k_0 > 0, \tag{42}$$

where

$$k_h = \inf_{q_h \in Q_h} \sup_{v_h \in V_h} \frac{b(v_h, q_h)}{\| v_h \|_V \| q_h \|_{Q/(KerB_h^t)}}. \tag{43}$$

Then there exists a solution (u_h, ρ_h) to the set of equations (34). The function u_h is uniquely determined in V_h, and ρ_h is uniquely determined to within an element of $Ker\ B_h^t$.

Some components of ρ_h might not be uniquely determined if $Ker\ B_h^t$ is larger than $Ker\ B^t$ (i.e., $Ker\ B_h^t \neq \{0\}$). These components appear as spurious modes in the solution. The key requirement for stability and convergence of the solution is that k_h should remain bounded away from zero ($k_h \geq k_0 > 0$) in the limit of mesh refinement; i.e., as $h \to 0$, where h is a measure of the size of an element. Note that satisfaction of the inf-sup condition does not guarantee a unique solution for ρ_h unless, $Ker\ B_h^t = \{0\}$. In some cases (e.g., when A is coercive on $Ker\ B$ and $Ker\ B_h \subset Ker\ B$), u_h remains a good approximation to u, even though spurious modes are present in ρ_h.

There are three strategies to deal with the possibility of spurious modes in the discrete solution. In the first strategy, we restrict our attention to finite element models that generate a unique solution. That is, we avoid spurious modes altogether. If n_u and n_ρ denote the dimensions of the vectors $\hat{u}$ and $\hat{\rho}$, then the requirements for obtaining a unique solution can be summarized as

i) $\boldsymbol{A}$ is positive definite in $Ker\ \boldsymbol{B}$; and

ii) $rank\ \boldsymbol{B} = n_\rho$.

Requirements *(i)* and *(ii)* above are discrete versions of the coercivity condition (equation (41)) and the inf-sup condition (equation (42)) when $Ker\ B_h^t = \{0\}$. The inequality $n_\rho \leq n_u$ is obviously a necessary condition for requirement *(ii)* to hold.

In the second strategy, we use a finite element model for which $Ker\ B_h^t \neq \{0\}$, but which still satisfies the coercivity and inf-sup conditions. Thus, spurious modes might appear in the solution for ρ_h, but the u_h solution is nonetheless a good approximation to the continuum solution u. Furthermore, ρ_h is a good approximation to the continuum solution ρ within an element of $Ker\ B_h^t$. If spurious modes do appear in the ρ_h solution, they can be filtered out using a postprocessing scheme [15]. In a few special cases, such as the bilinear velocity/ constant pressure element for the Stokes problem, reasonable results can be obtained by the postprocessing technique described above, even though the particular element does not satisfy the inf-sup condition [14]. However, in general, elements which do not satisfy the inf-sup condition are unreliable. The requirements for a unique solution $(u_h, \rho_h) \in V_h \times Q_h / Ker\ B_h^t$ can be summarized as

i) $\boldsymbol{A}$ is positive definite in $Ker\ \boldsymbol{B}$; and

ii) $\hat{\boldsymbol{g}} \in Im\ \boldsymbol{B}$.

In the third strategy, an augmented functional is introduced to stabilize the problem without affecting the solution. Hughes et al. present a Petrov-Galerkin formulation of the Stokes problem that stabilizes certain elements types which are unstable within the framework of the classical Galerkin formulation [17].

Unfortunately, even though the Stokes problem and problem P0i are both linear variational problems, the theoretical framework developed above for the Stokes problem cannot be applied directly to problem P0i. This is due to a fundamental difference between the structure of the two problems: the density fields ρ^0 and $\delta\rho$ in problem P0i must be in $L_\infty(\Omega)$ to ensure that the integrals in equations (15) and (16) are bounded, while in the Stokes problem we require the pressure field to be in $L_2(\Omega)$. Since $L_\infty(\Omega)$ is not a Hilbert space, the theoretical results presented above do not apply directly to problem P0i. However, the structure of the discrete problem P0d is identical to that of equation (38) when the functional in problem P0 is linear in ρ, so that $\boldsymbol{H} = \boldsymbol{O}$. The following section is devoted to a study of this special case.

4. Optimization problems with linear dependence on the distributed design parameter

We now consider optimization problems for which the design functional has a linear dependence on the distributed design parameter ρ. This implies that $\alpha = 0$ and that the strain energy density is a linear function of ρ. These restrictions ensure that we obtain $\boldsymbol{H} = \boldsymbol{O}$ in the discrete form of the incremental problem.

The compliance optimization of a variable-thickness elastic plate is a common application that is compatible with this restricted model. To illustrate, suppose that one dimension of the candidate domain, denoted t_{allow} and representing the maximum permissible thickness of the plate, is much smaller than the other dimensions of Ω. The thickness of the plate can be represented by the function, $t(\rho) = \rho t_{allow}$. That is, ρ is a distributed design parameter representing the thickness of the plate, normalized with respect to t_{allow}.

A differential volume is expressed as $dV = \rho d\Omega$. We assume a design-independent elasticity tensor $\boldsymbol{C}$ to obtain an *effective* strain energy density function (i.e., the strain energy per unit volume in Ω) that is linear in ρ: $W = \frac{\rho}{2}\varepsilon^t \boldsymbol{C}\varepsilon$. In keeping with this physical interpretation, we shall refer to this simplified problem as the *variable-thickness design problem.*

The following section describes the specialization of the development presented in Section 2 to the variable-thickness design problem. We describe the cause of the spurious modes that can generate grid-scale anomalies in finite element solutions to the incremental problem in Section 4.2. We also discuss the behavior of various finite element models. In Section 4.3, we describe a "patch test" that is useful for testing the stability of specific mixed finite element models for the variable-thickness problem.

4.1. Formulation of the variable-thickness design problem

We seek a density distribution, $\rho : \Omega \rightarrow \Re$, which minimizes the compliance of the structure such that the total volume of material equals a specified value $\bar{V}$. The variable-thickness design problem is obtained by substituting $\alpha = 0$ and $W(\varepsilon, \rho) = \frac{\rho}{2}\varepsilon^t \boldsymbol{C}\varepsilon$ into problem P0.

Problem P1:

Let ρ_{min}: $0 < \rho_{min} < 1$ and $\bar{V} > 0$ be given. Find $(\boldsymbol{u}^*, \rho^*) \in V_u \times V_\rho$ that solves

$$\sup_{\rho \in V_\rho} \quad \inf_{\boldsymbol{u} \in V_u} \quad \frac{1}{2}\int_\Omega (\varepsilon^t \rho \boldsymbol{C}\varepsilon)\, d\Omega - \int_{\Gamma_t} (\bar{\boldsymbol{t}} \cdot \boldsymbol{u})\, d\Gamma - \int_\Omega (\boldsymbol{b} \cdot \boldsymbol{u})\, d\Omega - \lambda\left(\int_\Omega \rho d\Omega - \bar{V}\right) \tag{44}$$

subject to $\rho_{min} \leq \rho \leq 1$ in Ω; where λ is the Lagrange multiplier associated with the constraint, $\int_\Omega \rho d\Omega = \bar{V}$.

The variational, incremental and discrete forms of the variable-thickness problem are obtained by making the corresponding substitutions into problems P0v, P0i and P0d. Ultimately, we obtain the discrete, incremental form of the variable-thickness problem:

Problem P1d:

Let ρ_{min}: $0 < \rho_{min} < 1$, $\bar{V} > 0$, $\hat{u}^0 \in \Re^{n_u}$ and $\hat{\rho}^0 \in \Re^{n_\rho}$: $\int_\Omega N_\rho d\Omega \hat{\rho}^0 = \bar{V}$ be given. Find

$(\delta\hat{u}, \delta\hat{\rho}) \in \Re^{n_u} \times \Re^{n_\rho}$ that solves

$$\begin{bmatrix} A & B^t \\ B & O \end{bmatrix} \begin{Bmatrix} \delta\hat{u} \\ \delta\hat{\rho} \end{Bmatrix} = \begin{Bmatrix} \hat{f} \\ \hat{g} \end{Bmatrix}, \tag{45}$$

subject to $\rho_{min} - \rho_\beta^0 \le \delta\hat{\rho}_\beta \le 1 - \hat{\rho}_\beta^0$; $\beta = 1, n_\rho$; where

$$A \equiv \int_\Omega B_u^t C B_u \rho^0 d\Omega, \tag{46}$$

$$B^t \equiv \int_\Omega B_u^t C B_u \hat{u}^0 N_\rho d\Omega, \tag{47}$$

$$\hat{f} = \int_{\Gamma_t} N_u^t \bar{t} d\Gamma + \int_\Omega N_u^t b d\Omega - B^t \hat{\rho}^0, \tag{48}$$

$$\hat{g} = \lambda \int_\Omega N_\rho^t d\Omega - \frac{1}{2} B \hat{u}^0, \tag{49}$$

and λ is the Lagrange multiplier associated with the constraint, $\int_\Omega N_\rho d\Omega \delta\hat{\rho}^0 = 0$.

Note that $\hat{g} = o$ corresponds to the uniform-strain-energy-density optimality condition, $\frac{1}{2}(\varepsilon^0)^t C \varepsilon^0 = \lambda$. Let n_ρ and n_u be the dimensions of $\delta\hat{\rho}$ and $\delta\hat{u}$, respectively. Then the conditions for obtaining a unique solution to equation (45) are summarized as

i) A is positive definite.

ii) $\quad rank\ \boldsymbol{B}^t = rank\ \boldsymbol{B} = n_\rho.$

Clearly, $n_\rho \leq n_u$ is a necessary condition for *(ii)* to hold. If $\boldsymbol{B}$ is not full rank, then spurious modes from $Ker\ \boldsymbol{B}^t$ can pollute the incremental solution. However, if requirement *(i)* is met, then the displacement solution can still be a reasonable approximation to the continuum solution. In physical terms, the spurious modes can be understood as design perturbations that generate zero pseudoloads and, therefore, zero changes in the displacement field.

4.2. *The cause of spurious modes and the behavior of specific finite element models*

We now describe the cause of spurious modes in the density solution, based on the two conditions presented above. First, we show that the coercivity requirement (condition *(i)*) is easily satisfied. The material stiffness matrix $\boldsymbol{C}$ is positive-definite, so $\boldsymbol{A}$ is positive-definite, provided that we satisfy $0 < \rho_{min} \leq \rho^0$ in Ω. Satisfaction of the coercivity condition then follows from the positive-definiteness of $\boldsymbol{A}$. Therefore, we need only verify condition *(ii)* to demonstrate the stability of a particular mixed finite element model. Note that $\boldsymbol{B}^t$ is a function of the current displacement estimate $\hat{\boldsymbol{u}}^0$. This dependence results from the nonlinear nature of problem P1, and does not occur in the Stokes problem. Thus, a particular mixed finite element model is stable if $\boldsymbol{B}^t$ is full rank for all admissible $\hat{\boldsymbol{u}}^0$; it is unstable if there exists a $\hat{\boldsymbol{u}}^0$ for which $\boldsymbol{B}^t$ is rank deficient. Although it is straightforward to determine the rank of $\boldsymbol{B}^t$ for a specific choice of $\hat{\boldsymbol{u}}^0$, it is difficult to formulate general results for an arbitrary $\hat{\boldsymbol{u}}^0$. Thus, it is far more difficult to establish the general stability of a finite element model for problem P1 than it is for the analogous Stokes problem.

We will use the *singular value decomposition* to investigate the rank of $\boldsymbol{B}^t$. The singular value decomposition of $\boldsymbol{B}^t$ is given by [18]

$$\boldsymbol{B}^t = \boldsymbol{U}\boldsymbol{S}\boldsymbol{V}^t, \tag{50}$$

where S is a pseudo-diagonal matrix containing the singular values of B, and U and V are matrices containing the left and right singular vectors respectively. B^t is rank-deficient when $r < n_p$, in which $r = rank\ B$. Assuming that the singular values are arranged in descending order in S, the last $n_p - r$ columns of V (corresponding to the $n_p - r$ zero singular values of S) form a basis for $Ker\ B^t$. These vectors, when they are present, are associated with the source of spurious modes in solutions to problem P1d.

We demonstrate below that the process of optimization itself can generate a $\hat{u}^0$ that makes B^t rank-deficient for some finite element models. First we review the performance of selected finite element models for the variable-thickness optimization problem.

Table 1 summarizes our numerical experience with certain mixed finite-element models for the compliance optimization problem. In the displacement interpolation column, Q4, Q8 and Q9 represent four-node, eight-node and nine-node quadrilateral displacement elements. In the density interpolation column, Q4 and Q4D represent bilinear continuous and bilinear discontinuous interpolations, respectively. UD represents a piecewise uniform density model that is discontinuous across element boundaries. Checkerboard patterns appear when the Q4/UD element is used with the rank-2 microstructure model, but they do not appear when this element is used in the variable-thickness problem. The latter model is stable. (See Section 5 for further discussion of the unstable rank-2 microstructure model.)

We use a 2×2 Gauss quadrature integration scheme for the Q4 and Q8 elements and a 3×3 Gauss quadrature scheme for the Q9 elements. The same integration scheme is used for formulating the stiffness matrix and in the update scheme for the density field (see [1], [2] for details of the numerical algorithm). The use of inconsistent integration schemes can lead to spurious modes in elements that are otherwise stable. In particular, the use of a 2×2 integration scheme for the discrete form of the equilibrium equation and a one-point integration scheme for the discrete optimality criterion can result in checkerboard modes when the Q4/UD element is used to model problem P1.

Uniform energy density distributions have a special significance in compliance optimization problems, since solutions to problem P1 feature uniform energy density distributions in regions where the upper and lower bound constraints on the density field are inactive. The uniform energy density condition is only enforced in a weak sense in discrete formulations, and is not necessarily satisfied in a pointwise fashion. In iterative solution procedures, the critical uniform energy density distributions are not achieved until the final stages of the solution process.

In cases involving unstable finite element models, it is commonly observed that the design field is well behaved and free of anomalies during the early iterations of the solution process. During this phase, the solution remains regular and appears to be converging to a reasonable approximation of a continuous optimal design. However, just when the solution approaches the expected optimal design, spurious modes develop and the solution becomes unstable. Based on this numerical experience, we conjecture that weak satisfaction of the uniform energy density optimality criterion in the later iterations (i.e., $\hat{\boldsymbol{g}} \approx \boldsymbol{o}$) leads to a displacement solution $\hat{\boldsymbol{u}}^0$ that makes $\boldsymbol{B}^t$ rank-deficient for unstable finite element models. That is, the necessary conditions for a solution to the optimization problem are sufficient to cause a singular system matrix. According to this conjecture, an unstable finite element model could produce stable design increments in the early stages of an iterative optimization procedure when the optimality criterion is not satisfied. However, we would expect to see spurious modes develop in the later iterations, as the solution converges to the optimal design.

As an example, consider a rectangular domain of unit thickness subjected to a linearly-varying traction as shown in Figure 4. The material properties are $E = 2.1 \times 10^7$ psi and $\nu = 0.25$. The structure is discretized using a 5×4 mesh. We specify a volume fraction of 45%. Note that the upper and lower bound constraints on the density field ($0 \leq \rho \leq 1$) are inactive everywhere in the optimum design. If we use a Q4/UD element model, which our numerical experience shows to be stable, the lowest singular value of the matrix $\boldsymbol{B}^t$ stays bounded away from zero as the energy density becomes

uniform in the later iterations (see Figure 5). However, if we use the Q4/Q4 model, a combination which is known to be unstable, the lowest singular value tends to zero in the later iterations, as shown in Figure 6. In Figures 5 and 6, S_{min} represents the lowest singular value of $\boldsymbol{B}^t$ at a given iteration, $(S_{min})_0$ represents the lowest singular value for the initial design, and Ξ is a measure of the optimality criterion residual given by

$$\Xi = \sup_{\beta} \left| \frac{\lambda \int_\Omega N_{\rho\beta} d\Omega - \int_\Omega \frac{1}{2} \varepsilon^t \boldsymbol{C} \varepsilon N_{\rho\beta} d\Omega}{\lambda \int_\Omega N_{\rho\beta} d\Omega} \right| ; \beta = 1, n_\rho. \tag{51}$$

We have so far been unable to demonstrate that every displacement solution that satisfies the weak optimality condition will generate a rank-deficient matrix $\boldsymbol{B}^t$ for an unstable element model. However, we can demonstrate that the conjecture holds for a regular grid of Q4/Q4 elements whenever the optimal design involves a uniform strain state (as in the above example). Of course, a uniform strain state satisfies the uniform energy density criterion. We next present a proof of this special case of the conjecture.

We assume a uniform grid of Q4/Q4 elements and a uniform strain field, $\boldsymbol{B}_u \hat{\boldsymbol{u}}^0$. The matrix $\boldsymbol{B}^t$ is rank-deficient if there exists a density increment $\delta\rho \in V_\rho$ such that

$\int_\Omega \delta\rho d\Omega = 0$ and

$$v^t \int_\Omega \boldsymbol{B}_u^t \boldsymbol{C} \boldsymbol{B}_u \hat{\boldsymbol{u}}^0 \delta\rho d\Omega = 0 \quad \forall v^t \in \Re^{n_u}. \tag{52}$$

We now demonstrate the existence of a spurious mode pattern that satisfies the volume constraint locally within each element, and which makes $\boldsymbol{B}^t$ rank-deficient. If x and y denote the element natural coordinates, then an arbitrary increment of the density field in a given element can be represented as $\delta\rho = a_1 + a_2 x + a_3 y + a_4 xy$, in which a_i is a scalar constant. Each row of $\boldsymbol{B}_u^t$ has the polynomial form

$$[\,(b_1 + b_2 y) \qquad (b_3 + b_4 x) \qquad (b_5 + b_6 x + b_7 y)\,]\,. \tag{53}$$

The term $\boldsymbol{C}\boldsymbol{B}_u\hat{\boldsymbol{u}}^0$ in equation (52) is a 3×1 vector of constants, since the strain state is uniform by assumption. Hence, each component of the vector $\boldsymbol{B}_u^t\boldsymbol{C}\boldsymbol{B}_u\hat{\boldsymbol{u}}^0$ is of the form

$$c_1 + c_2 x + c_3 y. \tag{54}$$

If we set $a_1 = a_2 = a_3 = 0$, then we have $\int_\Omega \delta\rho\, d\Omega = 0$ and we see that $\delta\rho = a_4 xy$ is orthogonal over every element domain to each component of the vector $\boldsymbol{B}_u^t\boldsymbol{C}\boldsymbol{B}_u\hat{\boldsymbol{u}}^0$, given by equation (54). This proves condition (52), and hence the singularity of $\boldsymbol{B}^t$ for all $\hat{\boldsymbol{u}}^0$ that generate uniform strain states. The spurious mode $\delta\rho = a_4 xy$ corresponds to the "saddle" form instability shown in Figure 7. The plus signs denote positive perturbations to the density field, while the negative signs denote negative perturbations.

A similar analysis can be applied to the Q8/Q4 element, which numerical experience shows to be stable. Under the assumptions of a regular mesh and a constant strain field, each component of the vector $\boldsymbol{B}_u^t\boldsymbol{C}\boldsymbol{B}_u\hat{\boldsymbol{u}}^0$ for the Q8/Q4 element is of the form (compare with equation (54))

$$c_1 + c_2 x + c_3 y + c_4 xy + c_5 x^2 + c_6 y^2. \tag{55}$$

Design perturbations of the form $a_4 xy$ are not orthogonal to the function given in (55), so there is no spurious mode similar to the one described for the Q4/Q4 model. Of course, this argument does not constitute a proof of the stability of the Q8/Q4 element. Nonetheless, our numerical experience (Table 1) shows this element to be stable.

As a practical matter, we would like to have a simple test to determine whether a mixed finite element model for problem P1 is stable or unstable. A single example of a spurious mode, for a specific grid configuration and displacement vector $\hat{\boldsymbol{u}}^0$, is sufficient to show that a given model is unstable in general. However, it is much more difficult to show that a model is generally stable, since one has to show that spurious modes do not

exist for all possible combinations of grids and strain states. Therefore, it would be desirable to identify *critical* grid configurations and strain states which can be expected to generate spurious modes for unstable elements. We have found that all elements which we have identified as unstable (based on our numerical experience) generate a rank-deficient matrix $\boldsymbol{B}^t$ when applied on a regular grid to a uniform state of strain. We conjecture that these two conditions constitute a critical case which can be used to discriminate between stable and unstable elements. This conjecture is the basis of the "patch test" described in the following section. Experience with the Stokes problem [15] and the variable-topology design problem supports the conjecture that spurious modes are more prone to develop on regular grids than on distorted meshes.

4.3. The patch test for problem P1

We now describe a patch test for problem P1, based on the conjecture of the previous section, which can be used to discriminate between stable and unstable mixed finite element models. The test involves checking the full-rank condition for $\boldsymbol{B}^t$ under the (suspected) critical conditions of a uniform stress state on a regular grid.

To test the stability of a particular mixed finite element model, we subject a regular grid of elements with a uniform density distribution to three different stress states: *i*) uniform uniaxial stress σ_x, *ii*) uniform uniaxial stress σ_y, and *iii)* uniform shear stress τ_{xy}. These test conditions correspond to uniform strain states that also satisfy the weak uniform energy density optimality condition. It can be shown that if $\boldsymbol{B}^t$ is full rank under each of the above stress states, then it must be full rank for all uniform stress states. We solve the singular value problem, given by equation (50) for each of the three states. If $\boldsymbol{B}^t$ is rank deficient for any of them, then the element is unstable and the columns of $\boldsymbol{V}$ corresponding to the zero singular values of $\boldsymbol{S}$ identify spurious modes that might pollute the density solution. If $\boldsymbol{B}^t$ is full rank ($r = n_\rho$) in all three cases, then the element is stable, provided our conjecture is true.

Results for the patch test on selected element models under the three uniform stress states are summarized in Table 2. These tests were carried out on a 5×4 mesh of square elements. The notation "FR" designates elements for which $\boldsymbol{B}^t$ is full rank under all three of the test stress states; "RD" identifies elements for which $\boldsymbol{B}^t$ is rank deficient under at least one of the test loading conditions. The three numbers below the "RD" entries indicate the number of zero singular values (i.e., the number of spurious modes) for each test loading case. The different number of spurious modes for the σ_x and σ_y cases are due to the non-square mesh. Note that there are more spurious modes for the uniaxial stress cases than there are for the shear loading case. It is not necessary to carry out the patch test for the Q4/Q4D element, since it violates the necessary condition, $n_\rho \leq n_u$. Based on these results, one would expect the Q4/Q4, Q4/Q4D and Q8/Q4D elements to generate spurious modes and the remaining elements to give stable solutions. This is indeed found to be the case in our numerical experience, as summarized in Table 1.

Figure 7 shows the single spurious mode for problem P1 generated by the singular value decomposition in the uniform-shear-stress patch test for the unstable Q4/Q4 element. Within each element, this spurious mode has the same saddle form, $\delta\rho = kxy$, that we identified in our proof of the instability of this element in section 4.2.

5. Optimization problems with nonlinear dependence on the distributed design parameter

We now consider the general case in which the design functional in problem P0 is a nonlinear function of the distributed design parameter ρ ($\boldsymbol{H} \neq \boldsymbol{O}$). This nonlinearity arises whenever $\alpha > 0$ or the strain energy density W is a nonlinear function of ρ. We analyze the stability of discrete models and propose a patch test to identify unstable elements in Section 5.1. In Section 5.2, we present examples applications and explain the behavior of specific finite elements in the context of the theory presented in Section 5.1.

5.1. Conditions for the stability of solutions to problem P0d

In what follows, we assume that a strict optimum exists for the continuum problem P0. Note that problem P0 need not necessarily be a saddle-point problem. Denoting the discrete version of the design functional in equation (9) by L, the Kuhn-Tucker conditions for a strict optimum of problem P0d are

Stationary conditions:

$$\frac{\partial L}{\partial \hat{u}} = o, \tag{56}$$

$$\frac{dL}{d\hat{\rho}} = o. \tag{57}$$

Second-order conditions:

$$\frac{\partial^2 L}{\partial \hat{u} \partial \hat{u}} \text{ is positive definite,} \tag{58}$$

$$\frac{d^2 L}{d\hat{\rho} d\hat{\rho}} \text{ is negative definite.} \tag{59}$$

The stationary condition with respect to $\hat{u}$ (equation (56)) yields the usual equations of equilibrium (i.e., the discrete version of equation (10)). The stationary condition with respect to $\hat{\rho}$ yields the discrete version of the weak optimality criterion (11). Note that equation (57) involves the total derivative of L with respect to $\hat{\rho}$, which is equal to the partial derivative of L with respect to $\hat{\rho}$ when equation (56) is satisfied.

The matrix $\begin{bmatrix} A & B^t \\ B & H \end{bmatrix}$ in equation (45) is the Hessian of L with respect to the vector $(\hat{u}, \hat{\rho})$. Thus, the matrix $\frac{\partial^2 L}{\partial \hat{u} \partial \hat{u}}$ is identical to the stiffness matrix A. In most applications, the stiffness matrix is positive definite and the second-order condition given by (58) is automatically satisfied. Equation (59) is the critical condition governing the stability of finite

element models. To evaluate the total derivative $\frac{d^2L}{d\hat{\rho}d\hat{\rho}}$, we introduce the linear coordinate transformation:

$$\begin{Bmatrix} \hat{u}' \\ \hat{\rho}' \end{Bmatrix} = P \begin{Bmatrix} \hat{u} \\ \hat{\rho} \end{Bmatrix}, \tag{60}$$

where P is a nonsingular matrix given by

$$P = \begin{bmatrix} I & A^{-1}B^t \\ O & I \end{bmatrix}. \tag{61}$$

The Hessian matrix in the transformed system is given by

$$\begin{bmatrix} A & O \\ O & H' \end{bmatrix} = P^{-t} \begin{bmatrix} A & B^t \\ B & H \end{bmatrix} P^{-1}, \tag{62}$$

where $H' = H - BA^{-1}B^t$. The transformation (62) ensures that the original and transformed Hessians are equivalent matrices. Recalling that the columns of $-B^t$ are the pseudoload vectors corresponding to the elements of $\delta\hat{\rho}$ (i.e., $-B^t = A\frac{\partial \hat{u}}{\partial \hat{\rho}}$), we see that the transformation (60) defines the vector $\delta\hat{u}'$ so as to cancel the part of $\delta\hat{u}$ induced by $\delta\hat{\rho}$. In other words, $\frac{\partial \hat{u}'}{\partial \hat{\rho}} = O$. This has the effect of uncoupling $\delta\hat{u}'$ and $\delta\hat{\rho}'$, as seen in equation (62).

Working in the transformed system, we have $\frac{\partial}{\partial \hat{u}} = \frac{\partial}{\partial \hat{u}'}$ and $\frac{d}{d\hat{\rho}} = \frac{\partial}{\partial \hat{\rho}'}$ since $\frac{\partial \hat{u}'}{\partial \hat{\rho}} = O$. Accordingly,

$$\frac{\partial^2 L}{\partial \hat{u} \partial \hat{u}} = \frac{\partial^2 L}{\partial \hat{u}' \partial \hat{u}'} = A, \tag{63}$$

$$\frac{d^2L}{d\hat{\rho}d\hat{\rho}} = \frac{\partial^2 L}{\partial\hat{\rho}'\partial\hat{\rho}'} = \boldsymbol{H}'. \tag{64}$$

Therefore the second-order conditions for a strict optimum solution to problem P0d are given by

$$\boldsymbol{A} \text{ is positive definite,} \tag{65}$$

$$\boldsymbol{H}' \text{ is negative definite.} \tag{66}$$

The first condition is automatically satisfied in most applications, as explained above. If $\boldsymbol{H}$ is positive definite, equation (66) is clearly violated if $n_\rho > n_u$. We assume that $\boldsymbol{A}$ is positive definite and that $n_\rho < n_u$ from here on. Equation (66) is the key requirement for stability of discrete solutions. If $\boldsymbol{H}$ is negative definite, then equation (66) is clearly satisfied, since $-\boldsymbol{B}\boldsymbol{A}^{-1}\boldsymbol{B}^t$ is at least negative semidefinite. The implication is that when $\boldsymbol{H}$ is negative definite, all finite element models (with $n_\rho < n_u$ and $\boldsymbol{A}$ positive definite) are stable! Unfortunately, in most distributed parameter optimization problems and especially problems involving topology optimization, $\boldsymbol{H}$ is positive definite. Then, to achieve a stable model, the discretization must be such that $\boldsymbol{H}'$ is negative definite in the vicinity of the optimum solution. However, $\boldsymbol{H}'$ need not be negative definite everywhere since the conditions given by equations (65) and (66) only pertain to the optimum solution.

The stability conditions presented in Section 4 for problem P1 are consistent with conditions (65) and (66) for the general problem P0. Since $\boldsymbol{H} = \boldsymbol{O}$ in problem P1 and $\boldsymbol{A}$ is assumed positive definite, $\boldsymbol{H}' = -\boldsymbol{B}\boldsymbol{A}^{-1}\boldsymbol{B}^t$ is negative definite if and only if $\boldsymbol{B}$ is full rank. If $\boldsymbol{B}$ is rank deficient at a stationary point, then $\boldsymbol{H}'$ is rank deficient and a strict optimum solution is not obtained. The rank deficiency implies a lack of uniqueness for the density field in the incremental problem; however, the incremental displacement field is uniquely determined. This is in contrast to the case in which $\boldsymbol{H}'$ has one or more positive eigenvalues at a stationary point, a condition which implies that the stationary point is not an optimum in the discrete problem. In some cases, the positive eigenvalues are an artifact of a particular finite element discretization and do not reflect the nature of the underlying con-

tinuum problem. This situation can trigger spurious modes in the discrete solution which generate a lower value of the objective function than the expected discrete representation of the continuum solution. Note that in contrast to the case where $\boldsymbol{H} = \boldsymbol{O}$, these spurious modes involve both the density and displacement fields.

We now describe a patch test to detect spurious modes for the case where $\boldsymbol{H} \neq \boldsymbol{O}$. The test attempts to identify elements for which $\boldsymbol{H}'$ is not negative definite at a known optimum point of the continuum problem. The test involves checking the eigenvalues of $\boldsymbol{H}'$ for a regular grid of planar elements subjected to three uniform stress states: *i)* uniform uniaxial stress σ_x, *ii)* uniform uniaxial stress σ_y, and *iii)* uniform shear stress τ_{xy}. The continuum optimum design (i.e., the uniform design field that satisfies the volume constraint) is assigned to each element. If any non-negative eigenvalues are detected, then the element is unstable. We conjecture that a regular grid and the three uniform stress fields comprise the critical cases for detecting spurious modes. Under this conjecture, any element for which all of the eigenvalues of $\boldsymbol{H}'$ are negative in all three cases is assumed to be stable in general. Although we do not have a proof for this conjecture, our numerical experience indicates that the proposed patch test is effective—all elements which appear to be stable in practice pass the test; while all elements which have been observed to generate spurious modes also exhibit positive eigenvalues in the patch test.

5.2. *Example applications for the general case of problem P0*

We now present a number of applications in which the Lagrangian exhibits a nonlinear dependence on ρ to illustrate the general case of problem P0 where $\boldsymbol{H} \neq \boldsymbol{O}$. In particular, we focus on formulations that are commonly used in variable-topology shape optimization. We discuss the behavior of various finite element discretizations for each application and illustrate the use of the patch test described in the previous section.

The penalized variable-thickness design problem

Our objective is to obtain a solution to the variable-topology design problem that consists primarily of solid and void material. We select a penalty parameter, $\alpha > 0$, in problem

P0 to approximate a 0-1 integer version of the variable-thickness optimization problem. Although the compliance remains linear in ρ ($W = \frac{\rho}{2}\varepsilon^t C\varepsilon$), the quadratic form of the penalty term generates a non-zero matrix $\boldsymbol{H}$. The matrix equations for the penalized problem are given by equation (25), with $\boldsymbol{A}$, $\boldsymbol{B}^t$ and $\hat{f}$ given by equations (46)-(48), and $\boldsymbol{H}$ and $\hat{\boldsymbol{g}}$ given by

$$\boldsymbol{H} = 2\alpha \int_{\Omega} N_\rho^t N_\rho d\Omega, \tag{67}$$

$$\hat{\boldsymbol{g}} = \lambda \int_{\Omega} N_\rho^t d\Omega - \frac{1}{2}\boldsymbol{B}\hat{\boldsymbol{u}}^0 + \alpha \int_{\Omega} (1 - 2\rho^0) N_\rho^t d\Omega. \tag{68}$$

Solutions to the unpenalized variable-thickness problem will, in general, contain regions where $\rho_{min} < \rho < 1$. As the parameter α is increased, the penalty on intermediate values of ρ becomes stronger. Eventually, for $\alpha \gg 0$, the upper and lower bound constraints on ρ are active almost everywhere in Ω. In this case, a solution to the continuum problem P0 does not exist, since V_ρ is not closed under the introduction of fine-scale oscillations in ρ [8]. Assuming that α is small enough to ensure the existence of a continuum solution, the stability of a discrete model is determined by the signs of the eigenvalues of $\boldsymbol{H}'$. A model which is stable for the unpenalized problem can be unstable under penalization. For example, the Q4/UD element, which is stable for problem P1, presents a checkerboard mode when the penalty term is added. Rozvany et al. [7] also report checkerboard modes for the Q4/UD element for the penalized variable-thickness problem.

An implicit penalty on intermediate densities

Sometimes the material model is manipulated to obtain an implicit penalty on intermediate values of ρ, as an alternative to the explicit penalty in the previous example. We set $\alpha = 0$ and define the strain energy to have a nonlinear dependence on ρ, the latter feature leading to a nonzero $\boldsymbol{H}$. Mlejnek and Schirrmacher introduce an artificial relationship between the elastic modulus and the density of the form [19]

$$C_{effective} = \rho^p C, \tag{69}$$

in which $p > 1$. In this model, the implicit penalty derives from the fact that extreme values of ρ provide a larger specific stiffness than intermediate values. This model is similar to the one used by Weinans et al. in their simulation of bone remodeling [9]. The matrix equations for this model can be derived using equations (20)-(25), with the strain energy density given by $W(\varepsilon, \rho) = \frac{1}{2}\varepsilon^t \rho^p C \varepsilon$ and $\alpha = 0$.

For $p < 1$, extreme values of ρ are penalized and a continuum solution to problem P0 is guaranteed to exist. We also have that H' is guaranteed to be negative definite in the discrete problem, so that any reasonable finite element model will be stable. The case $p = 1$ corresponds to the unpenalized variable-thickness problem discussed in Section 4. For $p > 1$, a continuum solution might or might not exist. In particular, the solution will not exist for large values of ρ (similar to the case $\alpha \gg 0$ in the previous example). Of particular interest is the case where p is greater than 1 but small enough to guarantee the existence of a continuum solution. Now H is positive definite, so H' might be indefinite. We must examine the eigenvalues of H' to determine the stability of a given discrete model.

We carried out numerical studies of the Q4/UD and Q8/UD elements for $p = 1.01$ and $p = 1.05$. For $p = 1.01$, both elements generated smooth, stable solutions in our trial optimization problems. Consistent with this result, both elements passed the patch test (that is, H' is negative definite for all three uniform stress states) for $p = 1.01$. For $p = 1.05$, the Q8/UD element was stable in all trials, but the Q4/UD element exhibited spurious modes in some, but not all, cases. The patch test results were consistent with these findings: the Q8/UD element passed the patch test for all three stress states, while the Q4/UD element presented a positive eigenvalue in the uniaxial stress cases. It is worth noting that the Q4/UD model nonetheless generates stable solutions and a negative definite H' under a uniform isotropic stress state. Thus, the stability of a given element under a fixed value of p is shown to be problem-dependent.

The relaxed, variable-topology design problem using rank-2 microstructures

A well-posed form of the variable-topology design problem is obtained by expanding the design space to include periodic, perforated microstructures and using homogenization methods to compute effective material properties [8]. Rank-2 microstructures are known to attain the optimal energy bounds, so the design can be restricted to this class of microstructures without loss of generality. The introduction of a perforated microstructure naturally defines a bulk density ρ; homogenization and analytical optimization of the microstructure automatically generates an effective strain energy density W as a function of ρ (see ([1], [2] for details). Solid and void conditions are realized in the microstructure; no attempt is made to suppress intermediate values of ρ. The relaxed form of the variable-topology design problem corresponds to problem P0, with $\alpha = 0$ and $W(\varepsilon, \rho)$ given by

$$\begin{aligned} \text{mode-I:}\quad & W(\varepsilon, \rho) = \frac{E\,(\varepsilon_I^2 + 2\varepsilon_I\varepsilon_{II}\,(1-\rho+\nu\rho) + \varepsilon_{II}^2)}{2\,(1-\nu)\,(2-\rho+\nu\rho)} \\ \text{mode-II:}\quad & W(\varepsilon, \rho) = \frac{E\,(\varepsilon_I^2 - 2\varepsilon_I\varepsilon_{II}\,(1-\rho-\nu\rho) + \varepsilon_{II}^2)}{2\,(1+\nu)\,(2-\rho-\nu\rho)} \\ \text{mode-III:}\quad & W(\varepsilon, \rho) = \frac{1}{2}\rho E\varepsilon_I^2 \end{aligned} \qquad , \tag{70}$$

where ε_I and ε_{II} are the principal strains defined such that $|\varepsilon_I| > |\varepsilon_{II}|$, and E and ν are the Young's modulus and Poisson's ratio. The modes are identified using the ratio $k = \varepsilon_{II}/\varepsilon_I$ as

$$\text{mode-I:}\quad \frac{1+k}{1-\nu} < \rho \le 1, \tag{71}$$

$$\text{mode-II:}\quad \frac{1-k}{1+\nu} < \rho \le 1, \tag{72}$$

$$\text{mode-III:}\quad 0 \le \rho \le min\,(\frac{1+k}{1-\nu}, \frac{1-k}{1+\nu}). \tag{73}$$

A continuum solution to the relaxed problem is known to exist [8]. Therefore, any failure to achieve a negative definite $\boldsymbol{H}'$ matrix in the vicinity of the optimum can be attributed to spurious modes that arise as artifacts of the discretization. The Lagrangian is linear

in ρ in mode-III regions, so $\boldsymbol{H} = \boldsymbol{O}$ and the analysis of Section 4 applies. The functional is nonlinear in ρ in mode-I and mode-II regions, and $\boldsymbol{H}$ is positive definite. Thus, it is possible that $\boldsymbol{H}'$ will have some non-negative eigenvalues, indicating the presence of spurious modes. We next report the results of our numerical investigation of this case.

Previous numerical studies found that the Q8/UD, Q9/UD, Q8/Q4 and Q9/Q4 elements are stable for the rank-2 model, while the Q4/UD, Q4/Q4, Q4/Q4D, Q8/Q4D and Q9/Q4D elements are not ([1], [2], [20]). (The Q4/UD element suffers checkerboard modes, the Q8/Q4D and Q9/Q4D elements suffer saddle modes as in Figure 8. The Q4/Q4, Q8/Q4, Q9/Q4 elements also exhibit spurious modes. The Q4/Q4D element violates $n_\rho < n_u$.) We carried out the patch test with a uniform isotropic loading (to ensure mode-II conditions) and a uniform shear (to ensure mode-I conditions). Surprisingly, our patch tests produced some positive eigenvalues for all of the elements considered, indicating that none of these elements are stable! This finding prompted us to run more stringent tests on the Q8/UD, Q9/UD, Q8/Q4 and Q9/Q4 elements. We increased the number of optimization iterations relative to our previous experiments in which these elements appeared to be stable. Indeed, spurious modes did eventually appear in the solutions for all of these elements. However, they did not appear until after the design had apparently converged and after many more iterations than were needed to produce spurious modes in the Q4/UD, Q4/Q4, Q4/Q4D, Q8/Q4D and Q9/Q4D elements. This suggests that the Q8/UD, Q9/UD, Q8/Q4 and Q9/Q4 elements are only mildly unstable, a notion that is supported by the fact that they generate positive eigenvalues in the patch test that are smaller in magnitude than those produced by the other elements. Although the discovery of unstable modes for these elements is cause for some concern, they might still be useful in practice since the spurious modes are not easily activated. We next present an explanation of the finding that spurious modes typically do not develop until after the discrete solution appears to converge to a reasonable approximation of the continuum solution.

Figure 9 presents a problem in which checkerboard instabilities appear with the rank-2 model for both the Q8/UD and the Q9/UD elements. The solution first appears to converge

rapidly to the continuum solution, then remains roughly the same for a number of iterations, but ultimately diverges in the later iterations. (It is interesting to note that similar behavior is reported in studies of adaptive bone remodeling [9].) The continuum solution is well approximated after about 20 iterations, but the checkerboard instabilities are clearly evident only after approximately 150 iterations. $\boldsymbol{H}'$ is indefinite throughout the iteration history for both element types. Thus spurious modes could develop at any time. However, the magnitude of the gradient of the Lagrangian in the unstable subspace (defined by the eigenvectors associated with the positive eigenvalues of $\boldsymbol{H}'$) remains small and the spurious modes do not participate significantly in the solution until the later iterations. Note that the mechanism that delays the appearance of spurious modes here is distinct from the one which is operative in the $\boldsymbol{H} = \boldsymbol{O}$ case, where $\boldsymbol{H}'$ becomes rank-deficient only when the solution approaches the continuum optimum.

Figure 10 illustrates this behavior for the Q8/UD element applied to the problem shown in Figure 9. We introduce the parameter ς to measure the magnitude of the projection of the gradient vector $\boldsymbol{d}^k$ into the unstable subspace at iteration k:

$$\varsigma = \frac{\left[\sum_{\beta = 1}^{n_p} (\boldsymbol{d}^k \cdot \omega_\beta^k)^2 \right]^{1/2}}{\lambda |\Omega|}. \tag{74}$$

The index β ranges over n_p, the number of positive eigenvalues of $\boldsymbol{H}'$. The corresponding eigenvectors ω_β^k are assumed to be normalized to unit magnitude. In Figure 10, we see that ς remains small until the later iterations.

6. Strategies for obtaining stable solutions

We now discuss three strategies for obtaining solutions to the compliance optimization problem that are free of spurious modes. The first strategy involves a postprocessing operation to filter out spurious modes, the second employs stable finite element models which

exclude spurious modes, while the third involves modifying the functional to ensure the stability of a given finite element model.

Bendsøe, Diaz and Kikuchi [21] describe a post-processing scheme for the Q4/UD element that attempts to filter out the spurious checkerboard mode using an operator which acts over a patch of four neighboring elements. This effectively introduces a type of "super" element to the finite element formulation, and is similar to the scheme introduced by Johnson and Pitkaranta for Stokes flow problems ([15], pg. 211). Since an inf-sup condition similar to equation (42) has not been formulated for the optimization problem, a mathematical justification for this scheme is not yet available.

An alternative strategy is to use a stable finite element model, such as the Q4/UD element for problem P1 or the Q8/UD element for the implicit penalty model (if p is not too large). We have yet to find an element type which is stable for the relaxed form of the variable-topology design problem under all loading conditions, but the instability of the Q8/UD, Q9/UD, Q8/Q4 and Q9/Q4 elements is very mild; these elements perform as though stable for all practical purposes.

A third possibility is to modify the Lagrangian in problem P0 to ensure that $\boldsymbol{H}'$ is negative definite in the vicinity of the optimum solution without affecting the stationary points of the functional. We have yet to pursue this possibility, but Petrov-Galerkin formulations [17] and augmented Lagrangian methods [22] are possible means to achieve this goal. This approach would allow greater flexibility in the choice of discrete function spaces for distributed-parameter optimization problems, leading to more efficient and more robust finite element models.

7. Conclusions

The central thesis of this work is that the theory of mixed variational problems provides a useful framework for understanding the cause of grid-scale anomalies in distributed-parameter optimization problems. However, the analysis of mixed finite element models for these problems is complicated by their nonlinear nature. For a simple material

model (e.g., the variable-thickness model), it is possible to reduce the problem to a form similar to that of the Stokes problem by considering an incremental formulation. However, the structure of the incremental formulation is not identical to that of the Stokes problem, since the density field ρ is constrained to be in L_∞, which is not a Hilbert space. A criterion similar to the inf-sup condition for the Stokes problem, but based on the L_∞ space, is needed to prove the convergence of finite element approximations. Whether such a criterion can be formulated remains an open question. Although the standard theory does not apply to the incremental continuum problem, the structure of the corresponding matrix equations is identical to the form of those encountered in the Stokes problem.

Although we do not have a convergence proof for the discrete variable-thickness design problem, we can explain the cause of instabilities for certain element types. We have proposed a patch test based on the matrix equations of the discretized incremental formulation. Our experience shows that spurious modes do not develop in unstable models until the design approaches the optimum—even when the optimal strain distribution is not uniform. This suggests that it might be possible to demonstrate that weak satisfaction of the uniform-energy-density optimality criterion is sufficient to make the $\boldsymbol{B}$ matrix rank-deficient in unstable elements.

For the more general case of problem P0, in which the design functional is a nonlinear function of the density parameter ρ, the $\boldsymbol{H}'$ matrix governs the stability of finite element models. Even when a continuum solution exists, there might be discrete models for which $\boldsymbol{H}'$ is not negative definite in the vicinity of the optimum solution, a condition that supports the occurrence of spurious modes. A patch test, similar to the one proposed for the variable-thickness design problem, can identify unstable elements. However, for both versions of the patch test, a proof that the patch test conditions are indeed critical is needed to demonstrate conclusively that an element which passes the patch test is generally stable. Nonetheless, our numerical experience shows the patch tests to be reliable in predicting the stability properties of specific mixed finite element models.

Acknowledgment

The authors wish to thank Martin P. Bendsøe of the Mathematical Institute at the Technical University of Denmark for his encouragement and many helpful suggestions. The authors would also like to thank the following organizations for their support of this work. The National Science Foundation (U.S.A.), the Danish Research Academy, the Danish Technical Research Council (Program for Research on Computer-Aided Design), Cray Research, Inc. and the Center for Supercomputing Research and Development. Computations were performed on the Cray Y-MP at the National Center for Supercomputing Applications.

		Displacement interpolation		
		Q4	Q8	Q9
Density interpo-lation	UD	S	S	S
	Q4	U	S	S
	Q4D	U	U	S

S = stable; U = unstable

Table 1 Stability of mixed finite elements for Problem P1.

		Displacement interpolation		
		Q4	Q8	Q9
Density interpol-ation	UD	FR	FR	FR
	Q4	RD (5, 6, 1)	FR	FR
	Q4D	RD	RD (15, 16, 0)	FR

Table 2 Rank condition of mixed finite element models for problem P1.

List of figures

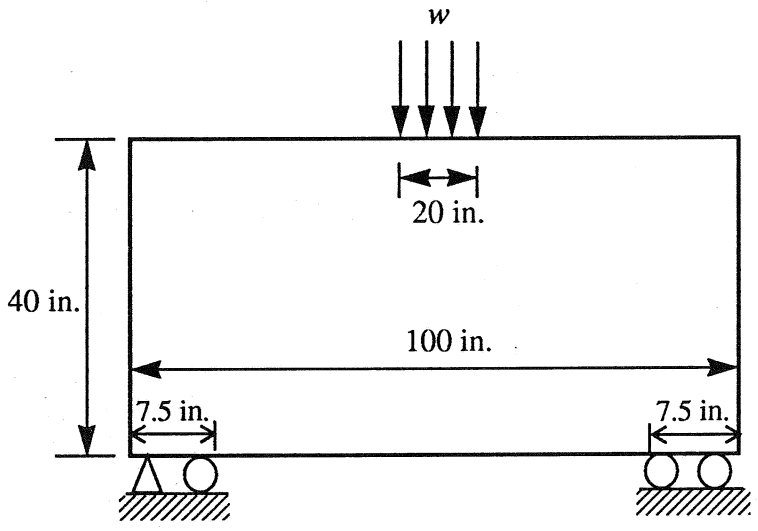

Figure 1 A rectangular design domain with a distributed load. The domain thickness is 1 in.; $w = 2.4 \times 10^4$ psi, $E = 2.1 \times 10^7$ psi and $\nu = 0.25$.

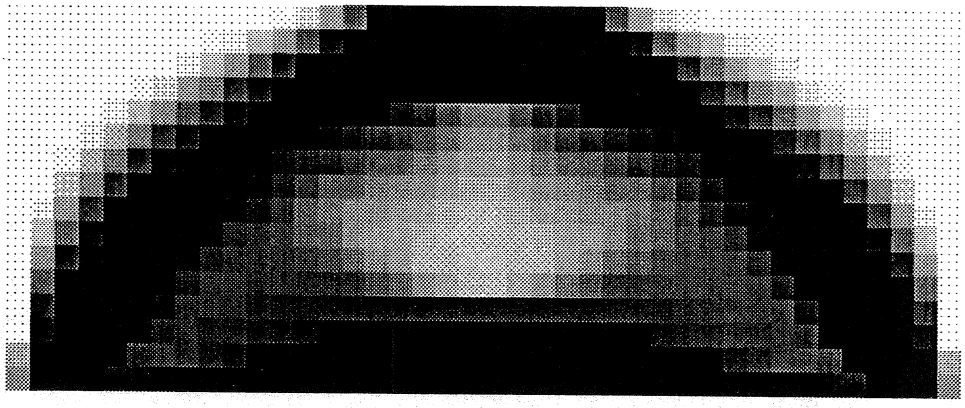

Figure 2 The bulk density distribution for the problem shown in Figure 1, obtained with 8-node displacement elements and uniform density per element.

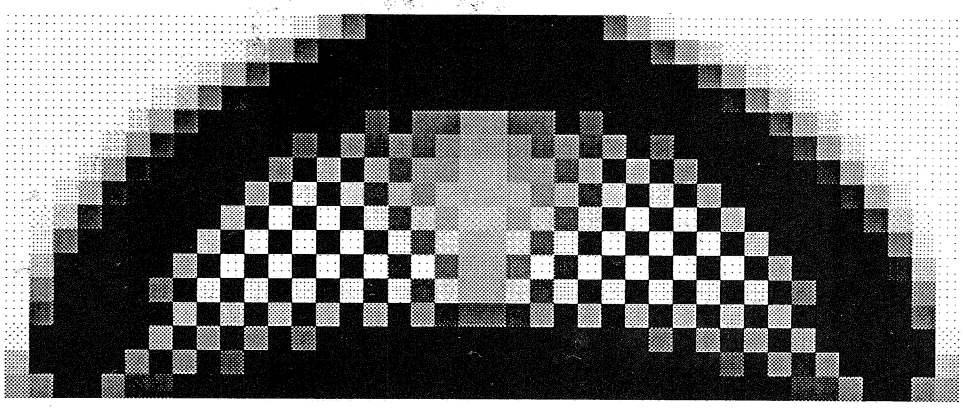

Figure 3 An unstable checkerboard solution for the problem shown in Figure 1, obtained with 4-node displacement elements and uniform density per element.

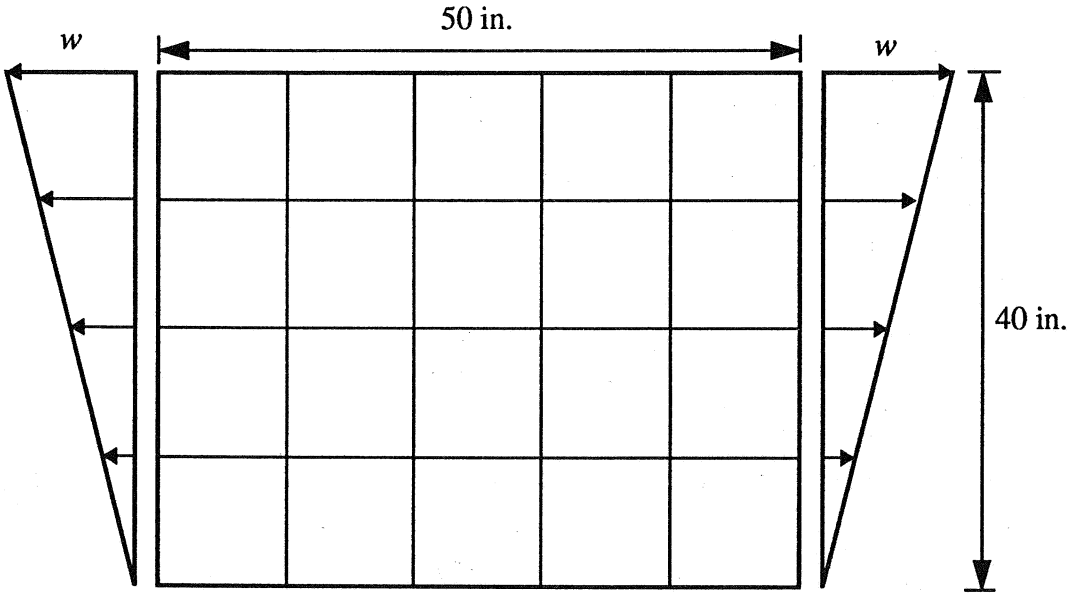

Figure 4 A rectangular domain subjected to a linearly-varying, distributed load ($w = 2.4 \times 10^4$ psi).

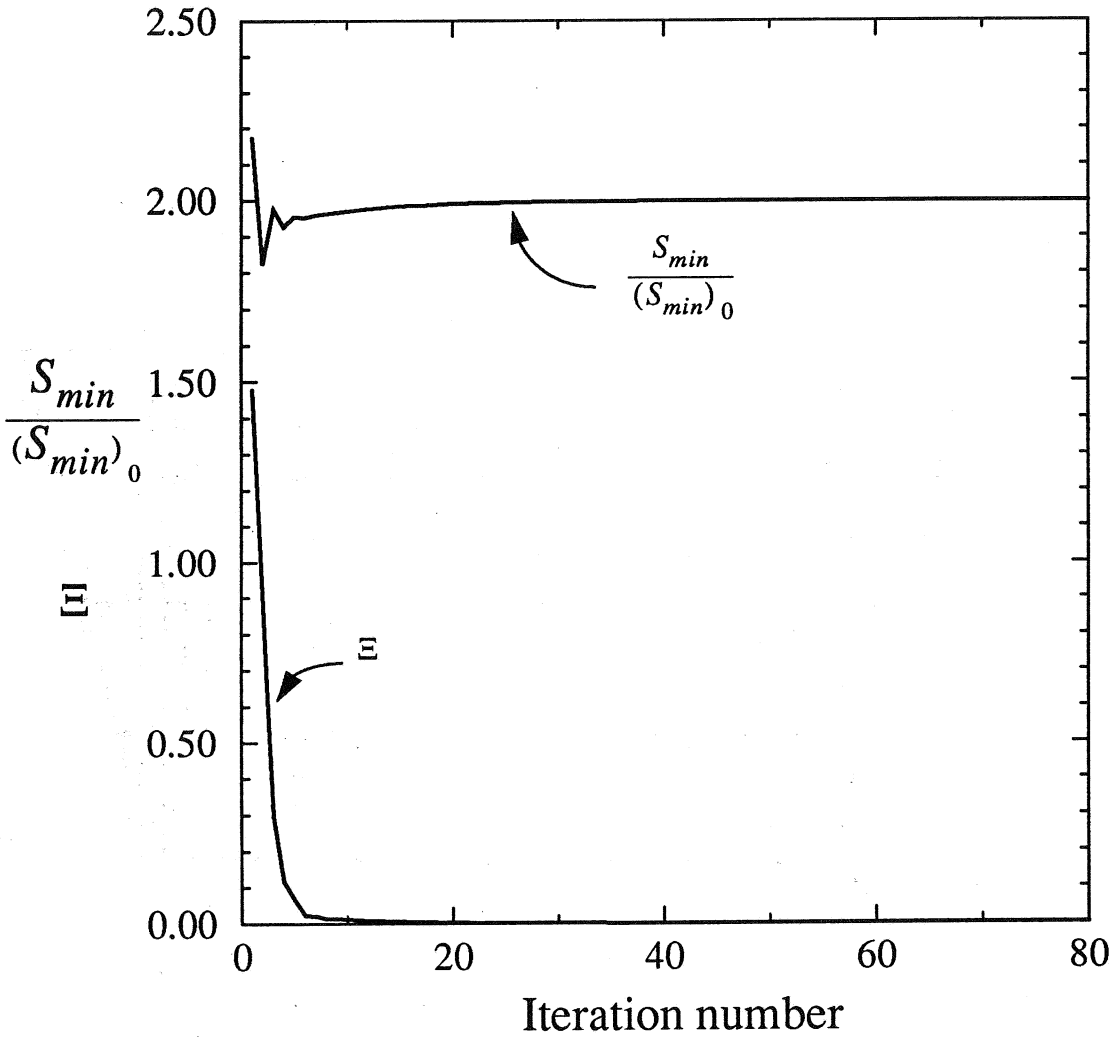

Figure 5 The lowest singular value of the matrix $\boldsymbol{B}^t$ and the parameter Ξ as a function of the iteration number for the Q4/UD element.

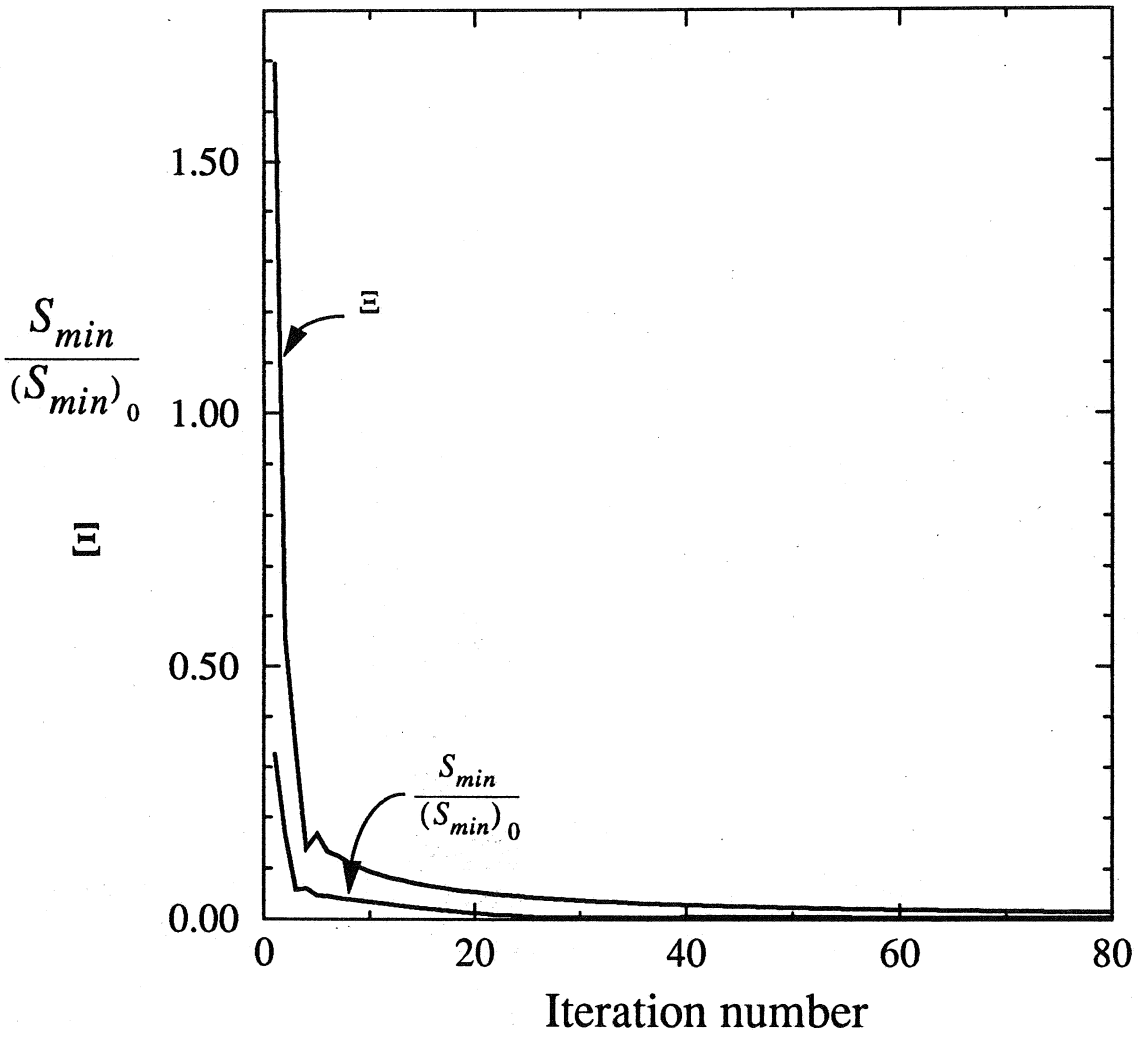

Figure 6 The lowest singular value of the matrix $\boldsymbol{B}^t$ and the parameter Ξ as a function of the iteration number for the Q4/Q4 element.

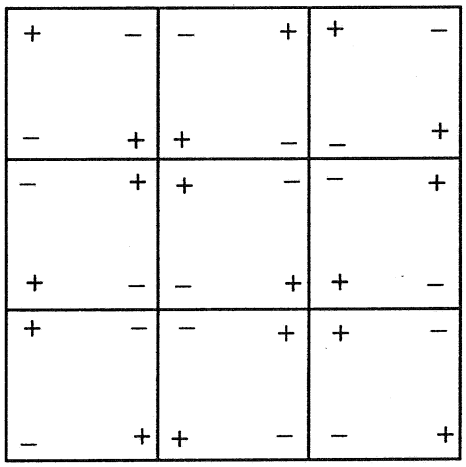

Figure 7 The spurious saddle mode for the Q4/Q4 element in problem P1.

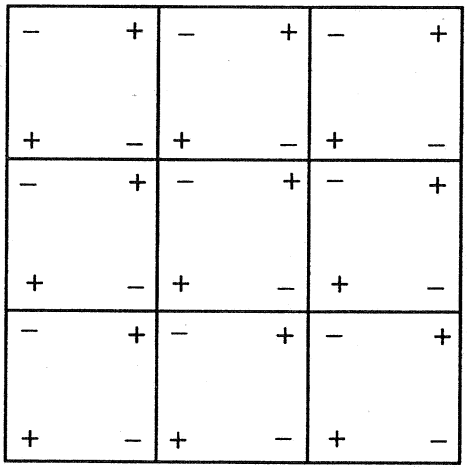

Figure 8 The spurious discontinuous saddle mode for the Q8/Q4D and the Q9/Q4D elements in problem P0 for the rank-2 microstructure model.

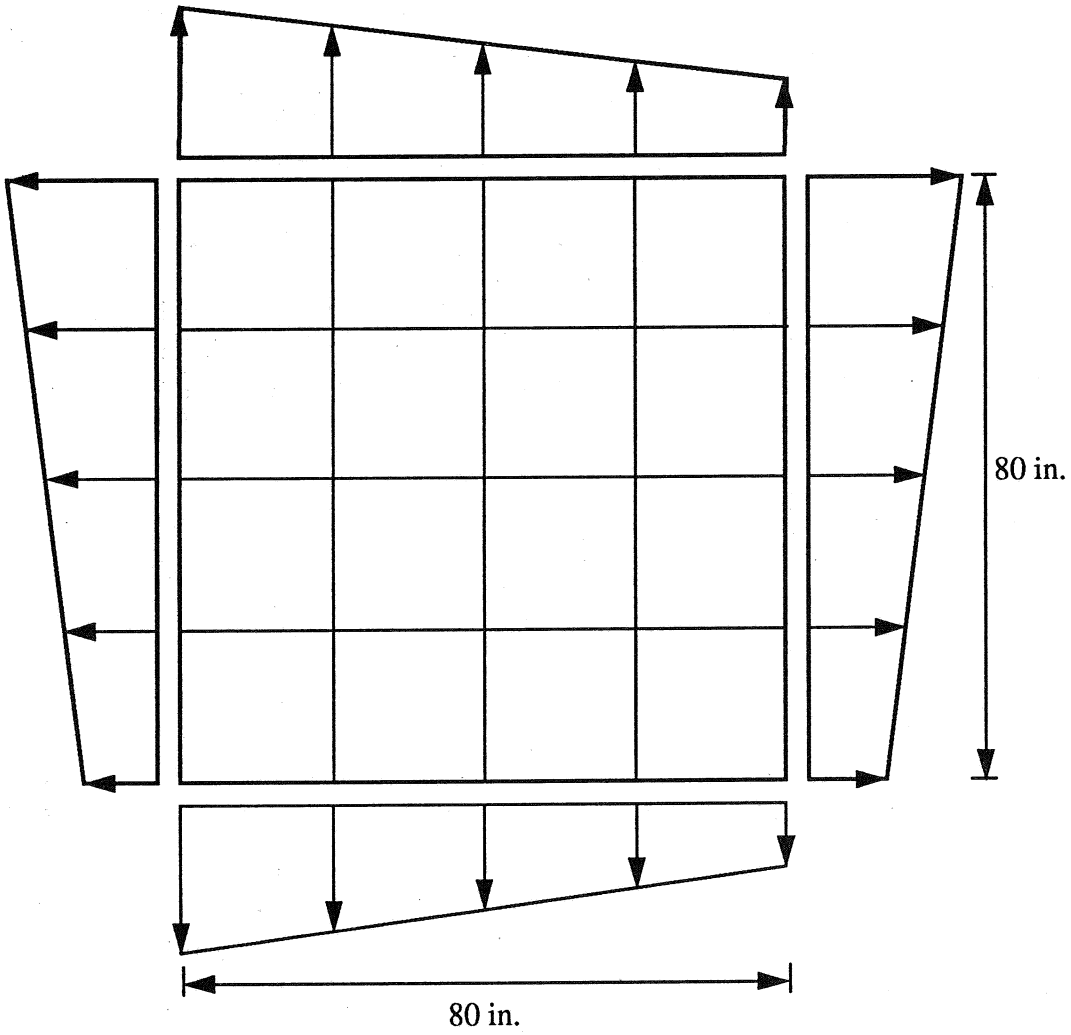

Figure 9 A square domain subjected to linearly-varying, distributed loads. The thickness is 1.0 in. and the maximum and minimum load intensities are 1.12×10^5 psi and 1.00×10^5 psi, respectively.

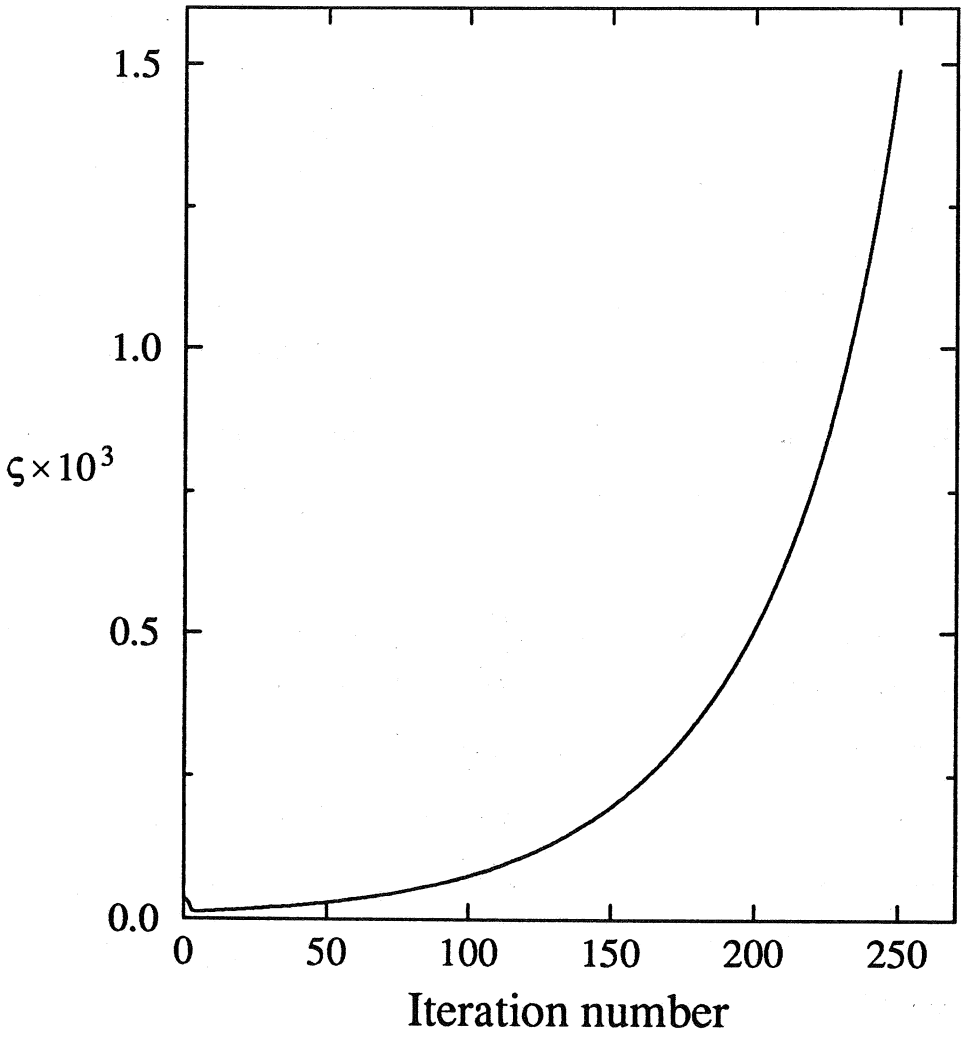

Figure 10 The parameter ς as a function of the iteration number for the Q8/UD element with the rank-2 microstructure model for the problem in Figure 9.

References

[1] C. S. Jog, R. B. Haber and M. P. Bendsøe, A displacement-based topology design method with self-adaptive layered materials, in: M. P. Bendsøe and C. A. Mota Soares, eds., Topology Design of Structures (Kluwer Academic Publishers, Dordrecht, The Netherlands, 1993) 219-238.

[2] C. S. Jog, R. B. Haber and M. P. Bendsøe, Topology design with optimized, self-adaptive materials, Int. J. Numer. Meth. Engrg. 37 (1994) 1323-1350.

[3] M. P. Bendsøe and N. Kikuchi, Generating optimal topologies in structural design using a homogenization method, Comput. Meth. Appl. Mech. Engrg. 71 (1988) 197-224.

[4] A. R. Diaz and N. Kikuchi, Solutions to shape and topology eigenvalue optimization problems using a homogenization method, Int. J. Numer. Meth. Engrg. 35 (1992) 1487-1502.

[5] N. Kikuchi and K. Suzuki, Structural optimization of a linearly elastic structure using the homogenization method, in: G. I. N. Rozvany, ed., Shape and Layout Optimization of Structural Systems and Optimality Criteria Methods, CISM Lecture Notes 325 (Springer Verlag, 1992) 199-242.

[6] K. Suzuki and N. Kikuchi, Generalized layout optimization of three-dimensional shell structures, in: D. A. Field and V. Komkov, eds., Geometric Aspects of Industrial Design (SIAM, Philadelphia, 1992) 62-88.

[7] G. I. N. Rozvany, M. Zhou, T. Birker and O. Sigmund, Topology optimization using iterative continuum-type optimality criteria (COC) methods for discretized systems, in: M. P. Bendsøe and C. A. Mota Soares, eds., Topology Design of Structures (Kluwer Academic Publishers, Dordrecht, The Netherlands, 1993) 273-286.

[8] R. V. Kohn and G. Strang, Optimal design and relaxation of variational problems, Comm. Pure Appl. Math. 39 (1986) 1-25 (Part-I), 139-182 (Part-II) and 353-377 (Part-III).

[9] H. Weinans, R. Huiskes and H. J. Grootenboer, The behavior of adaptive bone-remodeling simulation models, J. Biomechanics 25, No. 12 (1992) 1425-1441.

[10] S. A. Goldstein, S. J. Hollister, J. L. Kuhn and N. Kikuchi, The mechanical and remodeling properties of trabecular bone, in: V. C. Mow, A. Ratcliffe and S. L.-Y. Woo, eds., Biomechanics of diarthroidal joints, Vol. II (Springer, New York, 1990) 61-81.

[11] G. Allaire and G. A. Francfort, A numerical algorithm for topology and shape optimization, in: M. P. Bendsøe and C. A. Mota Soares, eds., Topology Design of Structures (Kluwer Academic Publishers, Dordrecht, The Netherlands, 1993) 239-248.

[12] R. B. Haber, C. S. Jog, M. P. Bendsøe, Variable-topology shape optimization with a control on perimeter, Proceedings, Twentieth ASME Design Automation Conference (Minneapolis, Minnesota, to appear).

[13] C. S. Jog, Variable-topology shape optimization of linear elastic structures, Doctors Thesis, University of Illinois at Urbana-Champaign, 1994.

[14] M. Fortin, Old and new finite elements for incompressible flows, Int. J. Numer. Meth. Fluids 1 (1981) 347-364.

[15] F. Brezzi and M. Fortin, Mixed and Hybrid Finite Element Methods (Springer-Verlag, 1991).

[16] E. J. Haug, K. K. Choi and V. Komkov, Design Sensitivity Analysis of Structural Systems (Academic Press, New York, 1986).

[17] T. J. R. Hughes, L. P. Franca and M. Balestra, A new finite element formulation for computational fluid dynamics: V. Circumventing the Babuska-Brezzi condition: A stable Petrov-Galerkin formulation of the Stokes problem accommodating equal-order interpolations, Comput. Meth. Appl. Mech. Engrg. 59 (1986) 85-99.

[18] P. Gill, W. Murray and M. Wright, Numerical Linear Algebra and Optimization, Vol. 1 (Addison-Wesley Publishing Company, 1991).

[19] H. Mlejnek and R. Schirrmacher, An engineering approach to optimal material distribution and shape finding, Comput. Meth. Appl. Mech. Engrg. 106 (1993) 1-26.

[20] H. C. Rodrigues and P. Fernandes, Topology optimization of linear elastic structures subjected to thermal loads, in: M. P. Bendsøe and C. A. Mota Soares, eds., Topology Design of Structures (Kluwer Academic Publishers, Dordrecht, The Netherlands, 1993) 437-450.

[21] M. P. Bendsøe, A. Diaz and N. Kikuchi, Topology and generalized layout optimization of structures, in: M. P. Bendsøe and C. A. Mota Soares, eds., Topology Design of Structures (Kluwer Academic Publishers, Dordrecht, The Netherlands, 1993) 159-205.

[22] M. Fortin and R. Glowinski, Augmented Lagrangian method applications to the numerical solution of boundary-value problems, in: J. L. Lions, G. Papanicolaou, R. T. Rockafellar, H. Fujita, eds., Studies in Mathematics and its Applications, Vol. 15 (North Holland, Amsterdam, 1983).

List of Recent TAM Reports

No.	Authors	Title	Date
708	Jog, C. S., R. B. Haber, and M. P. Bendsøe	Topology design with optimized, self-adaptive materials	Mar. 1993
709	Barkey, M. E., D. F. Socie, and K. J. Hsia	A yield surface approach to the estimation of notch strains for proportional and nonproportional cyclic loading	Apr. 1993
710	Feldsien, T. M., A. D. Friend, G. S. Gehner, T. D. McCoy, K. V. Remmert, D. L. Riedl, P. L. Scheiberle, and J. W. Wu	Thirtieth student symposium on engineering mechanics, J. W. Phillips, coord.	Apr. 1993
711	Weaver, R. L.	Anderson localization in the time domain: Numerical studies of waves in two-dimensional disordered media	Apr. 1993
712	Cherukuri, H. P., and T. G. Shawki	An energy-based localization theory: Part I—Basic framework	Apr. 1993
713	Manring, N. D., and R. E. Johnson	Modeling a variable-displacement pump	June 1993
714	Birnbaum, H. K., and P. Sofronis	Hydrogen-enhanced localized plasticity—A mechanism for hydrogen-related fracture	July 1993
715	Balachandar, S., and M. R. Malik	Inviscid instability of streamwise corner flow	July 1993
716	Sofronis, P.	Linearized hydrogen elasticity	July 1993
717	Nitzsche, V. R., and K. J. Hsia	Modelling of dislocation mobility controlled brittle-to-ductile transition	July 1993
718	Hsia, K. J., and A. S. Argon	Experimental study of the mechanisms of brittle-to-ductile transition of cleavage fracture in silicon single crystals	July 1993
719	Cherukuri, H. P., and T. G. Shawki	An energy-based localization theory: Part II—Effects of the diffusion, inertia and dissipation numbers	Aug. 1993
720	Aref, H., and S. W. Jones	Chaotic motion of a solid through ideal fluid	Aug. 1993
721	Stewart, D. S.	Lectures on detonation physics: Introduction to the theory of detonation shock dynamics	Aug. 1993
722	Lawrence, C. J., and R. Mei	Long-time behavior of the drag on a body in impulsive motion	Sept. 1993
723	Mei, R., J. F. Klausner, and C. J. Lawrence	A note on the history force on a spherical bubble at finite Reynolds number	Sept. 1993
724	Qi, Q., R. E. Johnson, and J. G. Harris	A re-examination of the boundary layer attenuation and acoustic streaming accompanying plane wave propagation in a circular tube	Sept. 1993
725	Turner, J. A., and R. L. Weaver	Radiative transfer of ultrasound	Sept. 1993
726	Yogeswaren, E. K., and J. G. Harris	A model of a confocal ultrasonic inspection system for interfaces	Sept. 1993
727	Yao, J., and D. S. Stewart	On the normal detonation shock velocity–curvature relationship for materials with large activation energy	Sept. 1993
728	Qi, Q.	Attenuated leaky Rayleigh waves	Oct. 1993
729	Sofronis, P., and H. K. Birnbaum	Mechanics of hydrogen–dislocation–impurity interactions: Part I—Increasing shear modulus	Oct. 1993
730	Hsia, K. J., Z. Suo, and W. Yang	Cleavage due to dislocation confinement in layered materials	Oct. 1993
731	Acharya, A., and T. G. Shawki	A second-deformation-gradient theory of plasticity	Oct. 1993
732	Michaleris, P., D. A. Tortorelli, and C. A. Vidal	Tangent operators and design sensitivity formulations for transient nonlinear coupled problems with applications to elasto-plasticity	Nov. 1993
733	Michaleris, P., D. A. Tortorelli, and C. A. Vidal	Analysis and optimization of weakly coupled thermo-elasto-plastic systems with applications to weldment design	Nov. 1993

(continued on next page)

List of Recent TAM Reports (cont'd)

No.	*Authors*	*Title*	*Date*
734	Ford, D. K., and D. S. Stewart	Probabilistic modeling of propellant beds exposed to strong stimulus	Nov. 1993
735	Mei, R., R. J. Adrian, and T. J. Hanratty	Particle dispersion in isotropic turbulence under the influence of non-Stokesian drag and gravitational settling	Nov. 1993
736	Dey, N., D. F. Socie, and K. J. Hsia	Static and cyclic fatigue failure at high temperature in ceramics containing grain boundary viscous phase: Part I—Experiments	Nov. 1993
737	Dey, N., D. F. Socie, and K. J. Hsia	Static and cyclic fatigue failure at high temperature in ceramics containing grain boundary viscous phase: Part II—Modelling	Nov. 1993
738	Turner, J. A., and R. L. Weaver	Radiative transfer and multiple scattering of diffuse ultrasound in polycrystalline media	Nov. 1993
739	Qi, Q., and R. E. Johnson	Resin flows through a porous fiber collection in pultrusion processing	Dec. 1993
740	Weaver, R. L., W. Sachse, and K. Y. Kim	Transient elastic waves in a transversely isotropic plate	Dec. 1993
741	Zhang, Y., and R. L. Weaver	Scattering from a thin random fluid layer	Dec. 1993
742	Weaver, R. L., and W. Sachse	Diffusion of ultrasound in a glass bead slurry	Dec. 1993
743	Sundermeyer, J. N., and R. L. Weaver	On crack identification and characterization in a beam by nonlinear vibration analysis	Dec. 1993
744	Li, L., and N. R. Sottos	Predictions of static displacements in 1–3 piezocomposites	Dec. 1993
745	Jones, S. W.	Chaotic advection and dispersion	Jan. 1994
746	Stewart, D. S., and J. Yao	Critical detonation shock curvature and failure dynamics: Developments in the theory of detonation shock dynamics	Feb. 1994
747	Mei, R., and R. J. Adrian	Effect of Reynolds-number-dependent turbulence structure on the dispersion of fluid and particles	Feb. 1994
748	Liu, Z.-C., R. J. Adrian, and T. J. Hanratty	Reynolds-number similarity of orthogonal decomposition of the outer layer of turbulent wall flow	Feb. 1994
749	Barnhart, D. H., R. J. Adrian, and G. C. Papen	Phase-conjugate holographic system for high-resolution particle image velocimetry	Feb. 1994
750	Qi, Q., W. D. O'Brien Jr., and J. G. Harris	The propagation of ultrasonic waves through a bubbly liquid into tissue: A linear analysis	Mar. 1994
751	Mittal, R., and S. Balachandar	Direct numerical simulation of flow past elliptic cylinders	May 1994
752	Anderson, D. N., J. R. Dahlen, M. J. Danyluk, A. M. Dreyer, K. M. Durkin, J. J. Kriegsmann, J. T. McGonigle, and V. Tyagi	Thirty-first student symposium on engineering mechanics, J. W. Phillips, coord.	May 1994
753	Thoroddsen, S. T.	The failure of the Kolmogorov refined similarity hypothesis in fluid turbulence	May 1994
754	Turner, J. A., and R. L. Weaver	Time dependence of multiply scattered diffuse ultrasound in polycrystalline media	June 1994
755	Riahi, D. N.	Finite-amplitude thermal convection with spatially modulated boundary temperatures	June 1994
756	Riahi, D. N.	Renormalization group analysis for stratified turbulence	June 1994
757	Riahi, D. N.	Wave-packet convection in a porous layer with boundary imperfections	June 1994
758	Jog, C. S., and R. B. Haber	Stability of finite element models for distributed-parameter optimization and topology design	July 1994